國立交通大學
光電工程學系暨研究所
博士論文

用飛秒時間解析激發-探測系統研究氧化鋅薄膜之超快光譜現象

Ultrafast Spectral Phenomena in ZnO Epitaxial Films by Using the Femtosecond Resolved Pump-probe

研究生：歐博濟
指導教授：謝文峰 教授

中華民國一百年九月

用飛秒時間解析激發-探測系統研究氧化鋅薄膜之超快光譜現象

Ultrafast Spectral Phenomena in ZnO Epitaxial Films by Using the Femtosecond Resolved Pump-probe

研 究 生：歐博濟　　Student: Po-Chi Ou

指導教授：謝文峰 教授　　Advisor: Prof. Wen-Feng Hsieh

國立交通大學

光電工程學系暨研究所

博士論文

A Dissertation
Submitted to Department of Photonics
And Institute of Electro-Optical Engineering
College of Electrical Engineering
National Chiao Tung University
In Partial Fulfillment of the Requirements
For the Degree of
Doctor of Philosophy
In
Electro-optical Engineering

September 2011
Hsinchu, Taiwan, Republic of China

中華民國一百年九月

用飛秒時間解析激發-探測系統研究氧化鋅薄膜之超快光譜現象

研究生：歐博濟　　　　指導教授:謝文峰　教授

國立交通大學光電工程學系暨研究所

摘要

以氧化鋅為基底的半導體材料，因其具有潛力做為藍光到紫外光波段的光電元件而備受重視。由於室溫下氧化鋅的激子束縛能約為60毫電子伏特，在氧化鋅的相關結構物中已經被觀察到光激發之受激輻射，包含激子與激子的散射與電子電洞的電漿型態。過去的文獻已經報導過氧化鋅薄膜中電漿形成及其受激放光的時間演化過程。此外，在時間解析螢光的研究中，大部分著重在載子的雷射動力學與激子的復合。對於了解氧化鋅中之超快載子動力學是必要的，因為這將有助於促進光增益與高速光電元件的發展。本論文中，我們利用了光學式激發-探測系統，研究室溫下氧化鋅薄膜的超快載子動力學，以及氧化鋅/氧化鎂鋅多層量子阱中的非線性光學吸收。

我們首先進行了室溫下吸收與螢光光譜的量測，藉此了解所使用樣品之線性光學特性。接下來，我們利用了標準激發-探測技術去量測 1 微米與 70 奈米氧化鋅薄膜的自由載子動力學。用瞬時反射量測的實驗結果表示，在 1 微米樣品中的自由載子熱化時間約為 1.0 至 1.5 皮秒，且隨著激發光能量的增加而增加。至於用瞬時穿透量測 70 奈米樣品的結果表示，觀測到較長的自由載子熱化時間約為 10 至 15 皮秒以及較緩慢的恢復時間。藉由比較這兩種不同薄膜厚度的結果，我們分析研究出厚度對於自由載子熱化時間的影響。受激自由載子將優先與薄膜表面發生碰撞，讓載子與聲子之間的碰撞機率降低，造成自由載子的熱化時間延長。由於 70 奈米樣品受到表面捕捉載子之效應，將造成受激載子的數量減少，

導致出現較緩慢的恢復時間。

在共振能量激發且強度為 10 μJ /cm^2 的條件下進行 70 奈米氧化鋅薄膜的瞬態穿透光譜量測，我們得到自由激子的超快鬆弛時間約在 1 皮秒之內，以及最大之吸收係數變化量為 1.8×10^4 cm^{-1}。我們進一步發現，自由激子的鬆弛時間將隨著光激發功率的增加而變短，這顯示著當激發功率增加時，激子的鬆弛行為將從激子與聲子的交互作用轉變為激子與激子的交互作用。由瞬態穿透光譜量測結果可以發現最大的瞬態穿透變化率恰好發生於自由激子的共振能階上。此外，在考量能帶填滿與能隙重整的物理機制下，我們使用模型理論去計算氧化鋅中折射率的變化量，進而成功地解釋了瞬態反射光譜之實驗結果。

除了研究氧化鋅薄膜之超快光譜現象，我們利用了開口式 Z 軸-掃描技術來量測氧化鋅/氧化鎂鋅多層量子阱中的非線性光學吸收。量測結果顯示，單光子飽和吸收效應發生於能量在靠近能隙與自由激子之間的區段，並隨著能量的降低而變大。受飽和吸收之影響，最大的非線性吸收係數發生於激子的共振能階上。當操作於波尾區段時，非線性吸收會開始發生雙光子吸收飽和特性。當我們的光激發波長操作在 375 奈米時，非線性吸收量測同時表現出單光子與雙光子飽和吸收之特性，而當波長操作於 378 奈米時，此特性逐漸轉為由雙子吸收飽和主導。

Ultrafast Spectral Phenomena in ZnO Epitaxial Films by Using the Femtosecond Resolved Pump-probe

Student: Po-Chi Ou　　**Advisor: Prof. Wen-Feng Hsieh**

Department of Photonics and Institute of Electro-Optical Engineering
National Chiao Tung University

Abstract

ZnO-based wide bandgap semiconductors have attracted much attention as a promising candidate for photonic devices in the blue to ultraviolet spectral region. Due to its large exciton binding energy of 60 meV at room temperature (RT), optically pumped stimulated emission from the exciton-exciton scattering and electron-hole plasma (EHP) have been demonstrated in ZnO related structures. There are some reports about temporal evolution of EHP formation and stimulated emission in ZnO thin films. Besides, most picoseconds time-resolved photoluminescence (PL) studies focused on the lasing dynamics and excitonic recombination, it is essential to understand the carrier dynamics and optical nonlinearities since they play important roles in realizing the optical gain process and developing ZnO-based photonic devices. Therefore, we investigated the ultrafast free carrier/exciton dynamics and nonlinear absorption in ZnO and ZnO/ZnMgO MQWs at RT in this thesis.

First, we measured the absorption spectrum and PL spectra at RT in the used samples to realize the linear optical properties. Then, we performed the free carrier dynamics in a 1-μm and a 70-nm ZnO epitaxial film by utilizing the standard

pump-probe technique. The results in a 1-μm sample show that ultrafast thermalization time around 1.0-1.5 ps increases slightly with increasing the excited photon energy by measuring the transient differential reflectance. As for the carrier dynamics in a 70-nm sample shows that prolonged thermalization time of 10-15 ps and slow recovery time for well-above band-gap states by measuring the transient differential transmission. By comparison of these two extremely thickness samples in order to investigate the thickness effect on ultrafast thermalization of free carriers for above band-gap states, the interaction between free carriers and sample surface induces the inefficient carrier–phonon scattering to result in the prolonged thermalization. And the loss of excited carrier density via surface trapping effect causes the slow recovery times in a 70-nm epifilm.

We also obtained the free exciton relaxation time to be less than 1 ps and the maximal differential absorption to be 1.8×10^4 cm^{-1} with pumping fluence of 10 μJ /cm^2 by demonstrating the free exciton dynamics in a 70-nm epifilm under resonant excitation. The relaxation time of free exciton decreases with increasing the pumping fluence that indicates the transition of relaxation from the exciton-phonon scattering into the exciton-exciton scattering. From the measurement of spectral dependent transient differential transmission, the largest induced transparency occurs at near exciton-resonance associated with absorption saturation. Moreover, based on a theoretical model to calculate the change of refractive index in ZnO, the measurement of spectral dependent transient differential reflectance can be successfully analyzed as a result of combination of band-filling (BF) and band-gap renormalization (BGR) effects.

In addition to the investigation of ultrafast spectral phenomena in ZnO thin films, we also utilized the standard open-aperture Z-scan method to measure the optical nonlinear absorption in ZnO/ZnMgO multiple quantum well structures (MQWs).

The saturation of one-photon absorption (OPA) increases as decreasing the excited photon energy from the conduction band-edge approaching the free exciton transition of ZnO QWs. The maximal nonlinear absorption coefficient can be observed near exciton resonance associated with absorption saturation. The contribution of the two-photon absorption (TPA) increases as tuning excitation in the shallow band-tail region. The characteristics of nonlinear absorption reveal the concurrence of OPA and TPA saturation for excitation wavelength at 375 nm, and gradually transit to the dominance of TPA as further increasing the photon wavelength at 378 nm.

誌　謝

回首過去這幾年的博士班生涯，的確是充滿了酸甜苦辣，這一段心路歷程能夠走到最後，也因為有許多人在身旁不斷地給予支持與鼓勵。首先，要感謝我的指導老師_謝文峰教授，老師用他過去幾十年的研究經驗，經常不厭其煩地與我們討論，一步一步帶領我去建構出研究的方向，分析所有我們觀察量測到的實驗數據，最後完成博士論文的撰寫。這裡也要特別感謝林家弘老師的大力協助，大部分的實驗都在北科光電完成，由於林老師以及他的學生的幫忙，讓所有實驗得以順利進行。志安陪我去參觀其他超快實驗室，合力讓我們的研究系統可以從無到有。立佐、厚傑、阿胖等學弟們陸續參與了超快的研究，陪同我一起找尋資料，改進研究的缺失，共同分析數據。也感謝其他北科的學弟們，在我跑台北做實驗的那兩年半的時間，在生活上的不方便上給予支援，讓我得以安心地在新竹-台北兩地奔坡進行實驗。一樣在念博士班的弟弟，除了為我加油打氣，也提供他的宿舍讓我跑台北的這段時間可以居住，並常與我分享他的經驗和方法。

攻讀博士班的這段期間，尤其要感謝我們雷射實驗室的這群好夥伴們。剛踏入實驗室時，有新翰、輝鴻、穎書、明容、小新、易慶等人的協助，他們邀約打球、聚餐及出遊，讓我快速融入了新的環境。智章學長指導我超快雷射的架設，在購買儀器及尋找論文主題時給予建議;小戴學長陪同我在電資大樓架設超快光學螢光系統;信民學長給了我一些寶貴的經驗，並提供我在染敏電池研究上的許多資訊。另外，感謝盧廷昌、刁維光老師以及孫建文老師提供他們實驗室的儀器資源，讓我得以更直接地去熟系超快光學系統。當然，要感謝的人少不了現在實驗室的同學，黃博、厚仁、智雅、小豪、小郭、張登登、誌軒、玠翰、松哥、碩哥、詮哥等，陪我度過許多下午茶時間、彼此分享與交流研究心得、討論實驗室的規劃、聊生活大小事、及免不了抱怨看不慣的事情，當然也組成了羽球及籃球的愛好會，用運動來增進我們之間的感情、放鬆研究的壓力。此外，謝謝我的室

友;以及博士班同學，芳正、俊毅、學姐，大家相約吃美食，彼此關照生活之所需。

此外，要感謝我學校社團的好夥伴們，有幸可以跟你們一起接觸禪修，從你們身上感受到許多感動的歡笑與淚水，並且可以在寒暑假去當志工或到中小學去服務，讓我的博士生涯更加充實;也感謝亭瑩這一段時間以來對我的包容與照顧。最後，要感謝我的父母，你們全然的付出，默默地為我鼓勵、支持與祝福，讓我可以沒有後顧之憂地去完成博士論文，能走過這一段歷程真的需要很多人的協助，將這一份喜悅分享給所有曾經關心過我的師長、家人及朋友。

Contents

List of Tables

List of Figures

Chapter 1 Introduction

Zinc oxide (ZnO), with wide band-gap energy of 3.37 eV and large exciton binding energy of 60 meV, has attracted much attention as a promising candidate for ultraviolet photonic devices. In this chapter, we introduce the room temperature optically pumped emission in ZnO epitaxial films including spontaneous emission and stimulated emission. We also discuss the mechanism of exciton-exciton scattering and electron-hole plasma. Finally, we give the research motivation and thesis structure.

1.1 Optical properties of ZnO

1.1.1 General merits of ZnO

There has been great interest in optical properties of zinc oxide (ZnO) with the wide band-gap energy of 3.37 eV for the development of ultraviolet photonic devices [1-5]. The natural structure of ZnO is a self-activated crystal, and it belongs to the II-VI compound and direct band-gap semiconductor. The wurtzite structure has a hexagonal unit cell with lattice constant of a = 3.2475 to 3.2501 Å and c = 5.2042 to 5.2075 Å. A schematic representation of the wurtzitic ZnO structure is revealed in Fig. 1-1 [6]. The structure is composed of two interpenetrating hexagonal-close-packed (hcp) sublattices, each consists of one type of atom displaced with respect to each other along the threefold c-axis by the amount of u in fractional coordinates. Each sublattice includes four atoms per unit cell and every atom of one kind (group-II atom) is surrounded by four atoms of the other kind (group VI), or vice versa, which are coordinated at the edges of a tetrahedron.

In the aspect of material growth, unintentionally doped ZnO is naturally n-type due to the presence of intrinsic defect such as Oxygen vacancies and Zinc interstitials.

Due to its exciton binding energy of 60 meV, larger than the room temperature (RT) thermal energy of 25 meV, free excitons can exist in ZnO even at RT [1-3]. Moreover, the exciton binding energy is larger than other wide band-gap semiconductors as shown in Fig. 1-2 , such as ZnSe (E^{b}_{ex} ~ 20 meV) and GaN (E^{b}_{ex} ~ 27 meV). Hence, ZnO is promising for exciton-based high efficiency and low threshold photonic device. Its transparency to visible light provides opportunities for developing transparent electrodes, UV optoelectronics, and integrated sensors. ZnO is also useful for a variety of practical applications, such as detectors [7], varistors [8], surface acoustic wave devices [9], hydrogen-storage devices [10], piezoelectric transducers, and window material for solar cells [11].

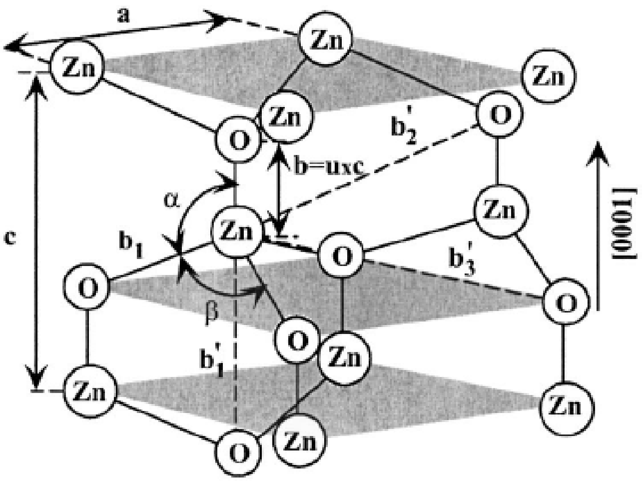

Fig. 1-1. Schematic representation of a wurtzite ZnO structure with lattice constants of a and c; u is the bond length. [6]

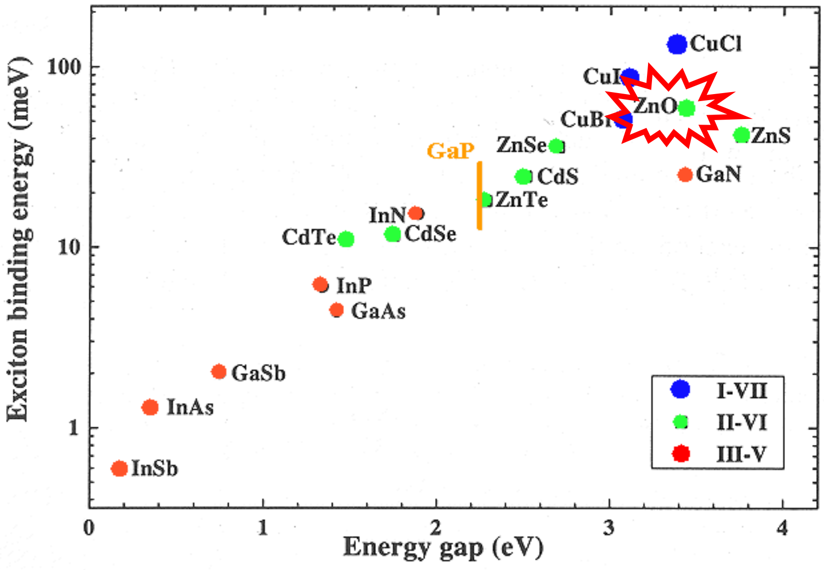

Fig. 1-2. The exciton binding energy E^b_{ex} as a function of the band-gap for various direct band-gap semiconductors.

1.1.2 Free exciton transition

An exciton, a Coulomb correlated electron-hole pair, can be visualized as a quasi-particle formed from a negatively charged electron in the conduction band and a positively charged hole in the valence band. The attractive Coulomb interaction binds these two constituents together to result in the exciton energy below the energy of a free electron-hole pair. In fact, there is a rather close physical analogy between the exciton and the hydrogen-like positronium atom that normal hydrogen atom theory is easily adapted to give a good description for exciton system by introducing the effective mass and dielectric constant. The excitons can be created through optical absorption with excited photon energies just below the band-gap.

Under the effective-mass approximation, the Coulomb interaction between electron and hole leads to a hydrogen-like problem with a Coulomb potential term $\frac{-e^2}{4\pi\varepsilon_0\varepsilon|r_e - r_h|}$. Excitons in semiconductors form, to a good approximation, a hydrogen or positronium like series of states below the band-gap. For a simple parabolic band in a direct band-gap semiconductor one can separate the relative motion of electron and hole and the motion of the center of mass. This leads to the dispersion relation of exciton [12], as shown in Fig. 1-3.

$$E_{\mathrm{ex}}(n_{\mathrm{B}}, \boldsymbol{K}) = E_{\mathrm{g}} - Ry^{*}\frac{1}{n_{\mathrm{B}}^{2}} + \frac{\hbar^{2}\boldsymbol{K}^{2}}{2M}, \qquad (1.1)$$

Here $n_B = 1, 2, 3\ldots$ is the principal quantum number, $Ry^{*} = 13.6\mathrm{eV}\frac{\mu}{m_0}\frac{1}{\varepsilon^{2}}$ is the exciton binding energy, $M = m_e + m_h$, and $K = k_e + k_h$ are the translational mass and wave vector of the exciton, respectively. The series of exciton states in Eq. (1.1) has an effective Rydberg energy Ry^{*} modified by the reduced mass of electron and hole and the dielectric constant of the medium in which these particles move.

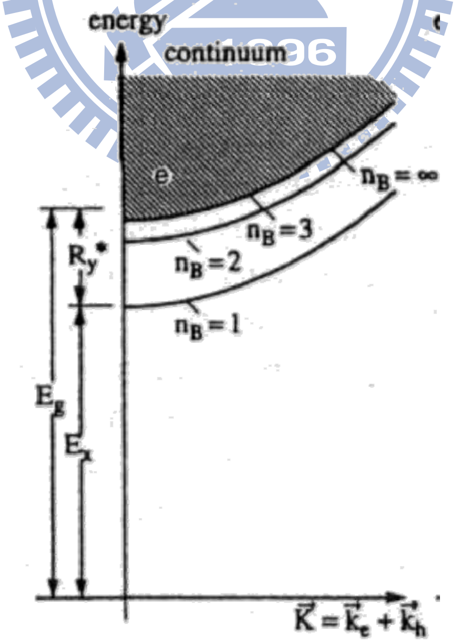

Fig. 1-3. A pair excitation in the scheme of valence and conduction band in the exciton picture for a direct gap semiconductor. [12]

The free exciton is a mobile particle capable of diffusing in the crystal, interacting with other excitons, and possibly becoming trapped at impurity sites before constituent electron-hole pair recombinations. The exciton can display properties similar to an atomic gas. It can bind with another exciton to form a bi-exciton, analogous to a hydrogen molecule. If a high density of excitons is created in a material, they can interact with one another to form an electron-hole liquid. The exciton Bohr radius of bulk ZnO is 2.34 nm. In the strong confinement regime, Senger et al. [13] demonstrated exciton radius in ZnO quantum dots changed dramatically as the crystal size closes to 2.34 nm.

1.1.3 Spontaneous emission

The exciton photoluminescence (PL), as a function of composition and structural peculiarities, is very sensitive to the crystal structures and the defects. Hence, the regularities of the change in exciton spectra can be used optically to determine the crystal quality. Generally speaking, room temperature PL spectra of ZnO typically consist of two bands. Figure 1-4 shows the spontaneous emission in a ZnO epitaxial layer at 295K [14]. The one in UV region corresponding to near-band-edge (NBE) emission is mainly contributed by free exciton states; the other one in the visible spectral range is due to the structural defects and impurities.

It has been reported the variations in the position of near band-edge emission in various ZnO nanostructures with relatively large dimensions are concerned with different concentration of native defects. Since the defect concentration on the sample surface is higher than in the bulk [15], spectral shifts are expected to occur in nanostructures with different sizes due to different surface-to-volume ratio. In addition, the defects could affect the shape of the luminescence spectra. Thus, the ratio of UV to defect emission can be useful in comparing the crystalline quality of different ZnO samples, when the PL measurements are performed under an identical excitation conditions.

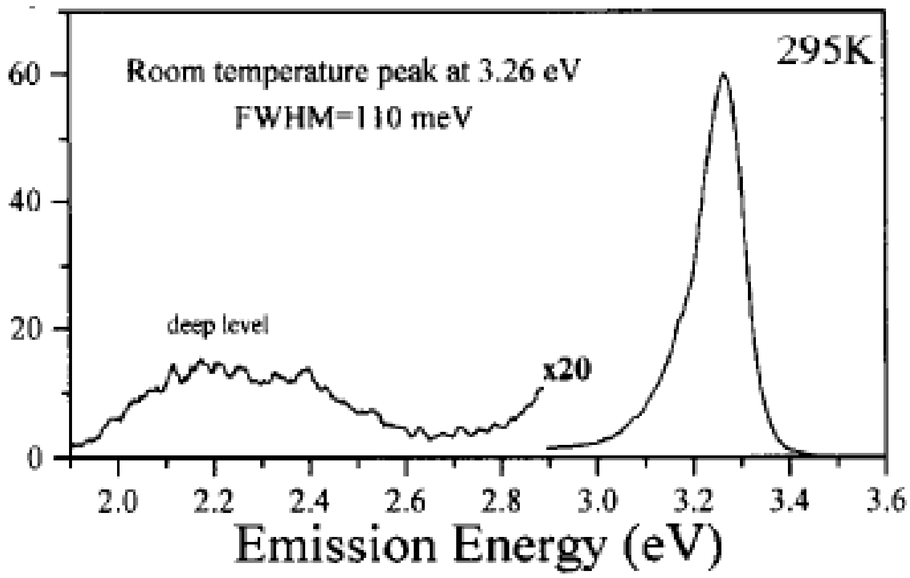

Fig. 1-4. The spontaneous emission including the UV and defect emission in ZnO. [14]

1.1.4 Stimulated emission

Due to its large exciton binding energy, ZnO has been attracted much attention for the achievement of excitonic stimulated emission at RT. Figure 1-5 shows the evolution of near band-edge emission spectra as the excitation intensity is increased from 198 kW/cm^2 to 1.32 MW/cm^2 [16]. Though the peak position is shifted to energies lower than the expected value at RT as a result of heating by the excitation laser, the PL spectra is mainly due to the free exciton emission when operated below 240 kW/cm^2. At this stage, the integrated emission intensity shows the linear dependence on excitation intensity corresponding to spontaneous emission process as shown in Fig. 1-6 [16]. When it was operated above 240 kW/cm^2, the rapid growth of a peak at 3.067 eV accompanied with the super-linear increase in output intensity and line-width narrowing from 214 to 73 meV can be observed. When the excitation intensity increased from 660 kW/cm^2 to 1.32 MW/cm^2, the output emission intensity increases tenfold and the peak position shifted to 3.032 eV.

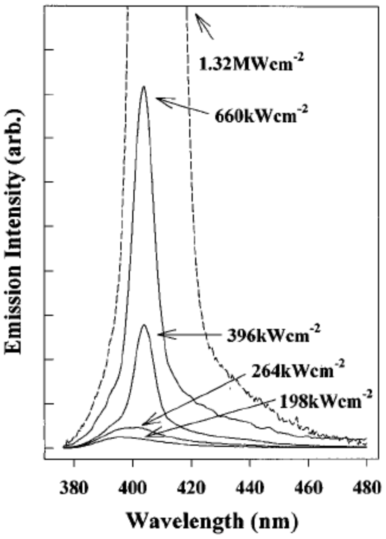

Fig. 1-5. The evolution of near-band-edge emission spectra at RT as the excitation intensity increased from 198 kW/cm^2 to 1.32 MW/cm^2. [16]

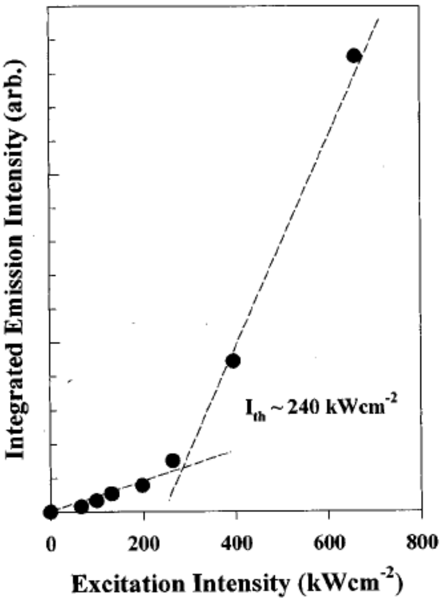

Fig. 1-6. The output integrated emission intensity with excitation intensity dependence at RT. [16]

Figure 1-7 shows the RT normalized PL emission spectra in a ZnO epilayer with thickness of 300 nm for various excitation intensities [17]. Under continuous wave He-Cd laser excitation, the emission peak position is close to the expected energy of the free exciton transition. As the excitation intensity increases to be larger than 400 kW/cm^2, a sharp stimulated emission peak emerges with photon energy at 3.18 eV and grows superlinearly. With further increase for excitation intensity above 800 kW/cm^2, a second peak emerges at 3.14 eV. This peak broadens and shifts to lower energy due to the band-gap renormalization.

The emission mechanisms of II–VI compounds under high excitation have been studied extensively. Stimulated emission in ZnO can be achieved either by exciton–exciton (EX-EX) scattering or electron-hole plasma (EHP) recombination. As the excitation intensity increases, exciton densities become sufficiently high to cause interaction. In the intermediate density regime, bi-excitonic, exciton–exciton, and exciton–carrier emissions may be observed. Bi-excitonic emissions are only observed at cryogenic temperatures. At higher temperatures exciton ionization increases the free carrier densities and an increasing probability of exciton–carrier emission. As the excitation power increases to achieve the intermediate regime, the increase in PL emission and the appearance of narrow lasing modes can be observed. At very high excitation intensities densities reach such levels that excitons overlap, the excitons lose their identity to become as individual quasi-particles and a new collective phase is formed. In this regime, the average distance of individual electron-hole pairs is comparable to or smaller than the Bohr radius and the PL spectra transits into the EHP emission. The lasing in these two excitation regimes will be discussed below.

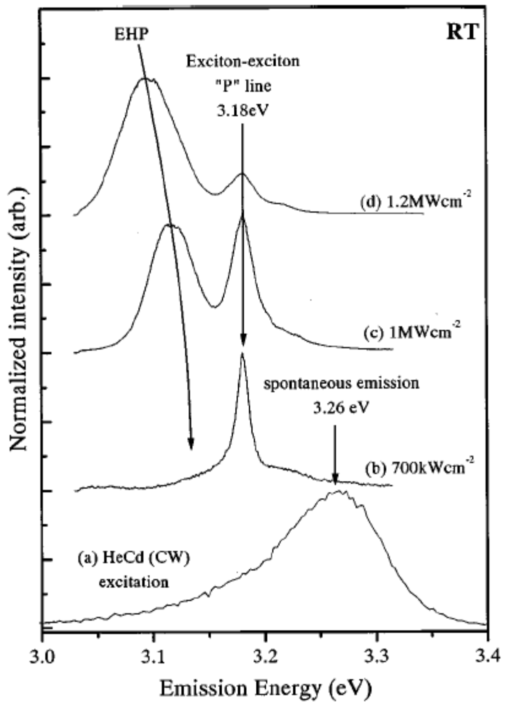

Fig. 1-7. Normalized PL spectra for various excitation intensities at RT. [17]

(a) EX-EX scattering

Figure 1-8 shows the inelastic exciton-exciton scattering process. As a result of such scattering process, one exciton is excited into a higher state (n = 2, 3, 4,..., ∞), while the other one loses its kinetic energy to occupy the lower polariton branch, whose energy can be given by [12, 18]

$$E_n = E_{ex} - E_{ex}^{b}(1 - 1/n^2) - 3k_B T/2, \tag{1.2}$$

where k_B is the Boltzmann constant, T is the temperature, and E_{ex}^{b} is the exciton binding energy. The transition from spontaneous emission to stimulated emission is evidenced by narrowing of the emission with a full-width half maximum (FWHM) about two orders of magnitude lower compared to the FWHM of spontaneous emission [19].

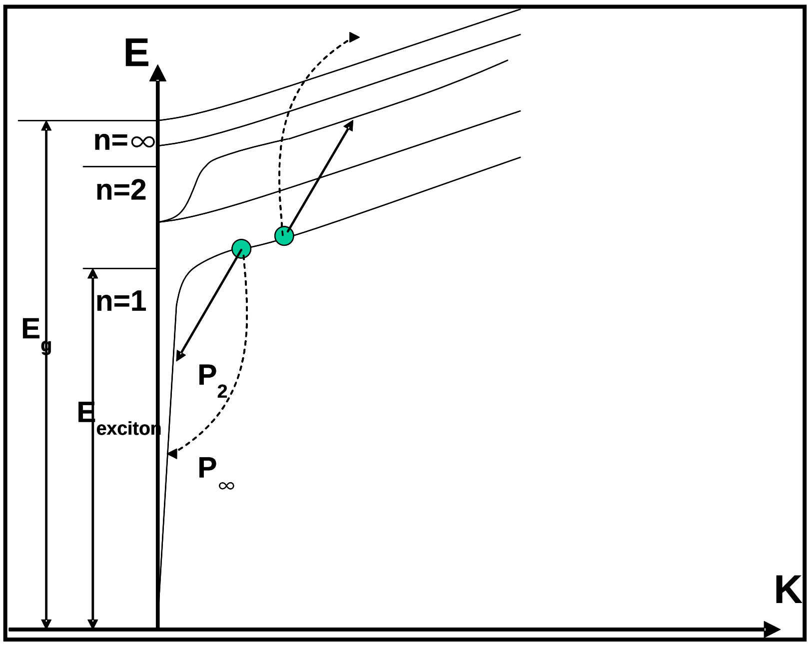

Fig. 1-8. Inelastic exciton-exciton scattering processes with excitation of intermediate density regime.

(b) Electron-hole plasma (EHP) emission

With increasing excitation intensity inside the sample, the excited density of excitons in ZnO will also increase. The electron-hole plasma (EHP) forms at densities higher than the Mott transition density: $n_M = \frac{kT}{2a_B^3 \cdot E_{ex}^b}$, where a_B is the Bohr radius [6]. This is estimated to be around 3.7×10^{19} cm^{-3} [6], although lower estimated value such as 4×10^{18} cm^{-3} [20] has also been reported. The EHP emission is typically broader accompanied with a red-shift when compared to stimulated emission from exciton–exciton scattering. The red shift of the EHP emission results from the band-gap renormalization effect [21]. Due to the spatial non-uniformity of the sample and the beam profile, the coexistence of these two mechanisms can be observed simultaneously in ZnO thin films [22]. Besides, the time-resolved PL studies in ZnO indicate that the coexistence may originate from the emergence of EHP state within a time delay of several picoseconds [23] followed by the stimulated emission from exciton-exciton scattering. After the decrease of excited carrier density through an EHP emission, the temporal evolution in stimulated emission spectra reveals a blue shift due to eventual recovery of renormalized band-gap.

1.1.5 Phonon replicas

LO-phonon replicas mean a polariton on the exciton-like part of the dispersion relation. An electron is scattered onto the photon-like branch by emitting one or more longitudinal optical phonons. The coupling with longitudinal optical phonon is stronger than that with transverse optical or acoustic phonons since the lattice distortion can be described largely as a superposition of longitudinal optical phonons. Phonon replicas in ZnO films have been reported for temperatures ranging from 50 to 250K.

In single crystals without defects, the emission peaks of 1-LO and 2-LO phonon replicas are shown to follow the theoretical expression:

$$E_{LO}^{m} = E_{ex} - m\hbar\omega_{LO} + (\frac{5}{2} - m)k_B T \quad , \tag{1.3}$$

where m is the number of phonon emitted, E_{ex} is free exciton transition energy, k_B is the Boltzman constant, $\hbar\omega_{LO}$ is the phonon energy, and T is the temperature. Low temperature PL spectrum of ZnO as shown in Fig. 1-9 indicates that 1LO-phonon replica of the free exciton labeled as 1LO (FX_A) is corresponding to photon energy around 3.306 eV [24]. The second and third order LO-phonon replicas labeled as 2LO (FX_A) and 3LO (FX_A) are also observed in the PL spectrum. It should be noted that LO-phonon replicas occur with a separation of 71–73 meV, apart from the peak energy of free exciton transition, corresponding to the optical phonon energy.

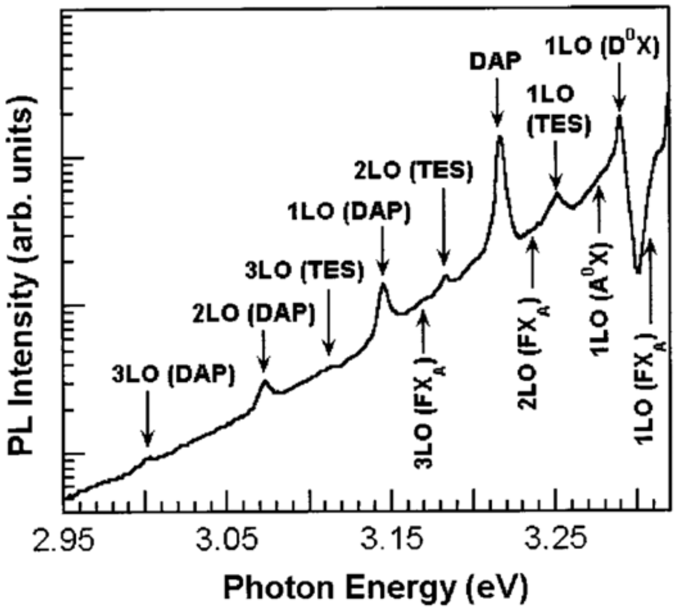

Fig. 1-9. Low temperature PL spectra at 10 K show the LO-Phonon replicas. [24]

1.2 Research motivation

During the past few years, advances in epitaxial growth with either plasma-assisted molecular-beam epitaxy (P-MBE) or pulsed laser deposition (PLD) on sapphire substrates have produced high quality ZnO epitaxial layers [16, 25]. The steady-state nonlinear absorption in near-IR and UV regions realize in our previous studies the detail optical information in ZnO by using the Z-scan method [26, 27]. Besides, previous literatures have reported that the Burstein-Moss effect reduces absorption, whereas the band-gap renormalization (BGR) effect normally induces absorption with photo-excitation above the band-gap states. Therefore, we demonstrate the spectral dependence of time-resolved photo-reflectance in ZnO epitaxial films to show the significance of competition of BF and BGR effects in this work.

Transient absorption measurements have been commonly performed in GaN and related III-V materials on time scales of femtosecond (fs) to nanosecond (ns) [28-30]. Recently, there were some reports about the carrier dynamics in ZnO [31-36], and most of the studies focused on the lasing dynamics and excitonic recombination by using the time-resolved PL. Under high excitation, Takeda et al. [33, 34] studied the transient EHP emission in ZnO by using the optical Kerr gate method. In their reports, the formation of EHP emerges with a delay time of 4-6 ps under band-to-band excitation; while it happens instantaneously under exciton resonant excitation. In order to realize the temporal evolution of free carriers convert into free excitons, we performed the carrier dynamics with excitation energy from the well-above band-gap states to the near exciton resonance by utilizing the standard pump-probe technique in ZnO at RT.

For the best performance of ZnO-based high speed photonic devices, it is imperative to understand the thickness effect on free carrier thermalization in ZnO epifilms since they play important roles in stimulated emission and gain process in real photonic device structures. By exciting the free carriers to the above band-gap states of two extreme thicknesses of epifilms, we compared the intra-band relaxation via carrier-phonon scattering against the interaction between the free carriers and the sample surface. Besides, we performed the carrier dynamics in a thick ZnO sample to directly monitor the ultrafast thermalization without taking surface trapping into account.

1.3 Organization of dissertation

In this thesis, we explored the ultrafast carrier dynamics in ZnO epitaxial films by using the femtosecond time-resolved pump-probe technique at RT. We observed the carrier dynamics with excitation from the above band-gap states to the band-tail states by measuring the transient differential transmission and reflectance. The thesis is organized as follows.

In Chapter 2, we introduce the background knowledge of ultrafast physical processes in semiconductors. We begin with some important scattering processes, in which the temporal evolution occurs in hundreds of femtoseconds to several picoseconds. Some important optical effects resulted from photo-excited carriers, such as the band-filling (or Burstein-Moss) effect and band-gap renormalization are discussed in detail. We also give some previous reports by using the optical Kerr gate method and the optical pump-probe technique, respectively. In Chapter 3, we describe the experimental instruments and setups, including the absorption spectral photometer and single grating monochromator, which can be useful to realize the absorption spectrum and time-integrated photo-luminescence spectra of prepared sample. In addition, the optical time-resolved system setup with two categories of transmission and reflection type pump-probe techniques was utilized to investigate the characteristics of ultrafast phenomena in ZnO materials.

In Chapter 4, we report the measurement of energy dependent ultrafast thermalization by using the pump-probe reflection. We also observed the transient reflectance with spectral dependence, which can be analyzed successfully with a model calculation for change of refractive index in ZnO. We compare the free carrier dynamics in the 70-nm (thin) and the 1-μm (thick) ZnO epifilms. The far above band-gap dynamics in the thin epifilm reveals the prolonged relaxation and the slow recovery of renormalized band-gap, while the far above band-gap dynamics in the thick epifilm reveals ultrafast relaxation. In Chapter 5, we measured the pumping dependent exciton relaxation by using the transmission pump-probe technique. The relaxation time and the saturation intensity can be obtained at near exciton resonance. In addition to the investigation of ultrafast spectral phenomena in ZnO thin films, the optical nonlinear absorption of ZnO/ZnMgO multiple quantum wells was performed in Chapter 6. Finally, we give the conclusions and the future works in Chapter 7.

Chapter 2 Theoretical background

To improve and to develop high-speed optoelectronic devices, there must be essential to understand various dynamical processes in the semiconductors of interest. However, most electronic instruments are not suitable to investigate ultrafast relaxation dynamics with time scale less than 10 ps. Fortunately, the generation of ultra-short laser pulse is capable of providing a way, known as optical pump-probe spectroscopy, to get insight into the ultrafast phenomena.

In this chapter, we first introduce the nonlinear optical effects including the band filling and the band-gap renormalization. Then, we introduce the temporal evolution in semiconductors and the method to achieve the ultrafast dynamics measurements. Finally, the review articles about ultrafast carrier dynamics in ZnO are discussed in detail by using the optical Kerr gate method and the transient absorption measurement.

2.1 Carrier-induced optical effects

In the following, we introduce nonlinear mechanisms induced by optical excitation that are the band-filling effect and the band-gap renormalization.

2.1.1 Band filling effect

The electrons and holes as Fermions can occupy each quantum state only once according to the Pauli exclusive principle. Hence each k state in a semiconductor band can be occupied twice, once with a spin-up and once with a spin-down carrier. An occupied state is no longer available as a final state in an optical absorption process. Due to the principle of energy minimization, the carriers in quasi-equilibrium occupy the available states from the bottom of the band, so that the energetically lowest states are occupied first. This results in filling the states near the bottom of the conduction band by electrons and the top of the valance band by holes. Hence, there is a decrease in the absorption coefficient at energies above the band-gap.

If parabolic bands are assumed or under the effective-mass approximation, the optical absorption near the band gap in a direct-gap semiconductor is given by the square-root law: $\alpha_0(E)=\frac{C}{E}\sqrt{E-E_g}, E\geq E_g$ and $\alpha_0(E)=0$ for $E\leq E_g$, where $E=\hbar\omega$ is the photon energy, E_g is the band-gap energy, and C is a constant involving material's parameters, matrix elements between periodic parts of the Bloch states at the band edges and the fundamental constants.

In the case of band filling, there is a finite probability that a state in the conduction band will be occupied by an electron and/or a state in the valance band will be empty (of electrons). If we denote an energy in the valance band by E_a and an energy in the conduction band by E_b, then the absorption coefficient of an injected semiconductor is

$$\alpha(N,P,E)=\alpha_0(E)[f_v(E_a)-f_c(E_b)], \tag{2.1}$$

Here N and P are the concentrations of free electrons and holes, respectively, α_0 represents the absorption of pure materials in the absence of injection, $f_c(E_b)$ is the probability of a conduction band state of energy E_b being occupied by an electron, and $f_v(E_a)$ is the probability of a valance band state of energy E_a being occupied by an electron. The change in absorption induced by the band filling is

$$\Delta\alpha(N,P,E)=\alpha_0(E)[f_v(E_a)-f_c(E_b)-1], \tag{2.2}$$

For the case of injection, we will have $f_c > 0$ and $f_v < 1$ close to the respective band edges. This formula predicts Δα is negative, i.e., the band filling decreases the absorption coefficient at a fixed incident photon energy. The real and imaginary parts of the refractive index $n+i\kappa$ (or dielectric constant $\varepsilon_1+i\varepsilon_2$) are related by Kramers-Kronig integrals:

$$n(E)=1+\frac{2c\hbar}{e^2}P\int_0^{\infty}\frac{\alpha(E')}{E'^2-E^2}dE', \tag{2.3}$$

where $\alpha=\dfrac{4\pi\kappa}{\lambda}$, c is the speed of light, e is the electron charge, E is the photon energy, and P indicates the Cauchy principal value of the integral. In analogy with the change of absorption coefficient we defined the change of refractive index as:

$$\Delta n(N,P,E)=n(N,P,E)-n_0(E), \tag{2.4}$$

where n_0 is the refractive index of un-injected material. The change in refractive index is then given by

$$\Delta n(N,P,E)=\frac{2c\hbar}{e^2}P\int_0^{\infty}\frac{\Delta\alpha(N,P,E')}{E'^2-E^2}dE'. \tag{2.5}$$

The refractive index decreases for energies near and below E_g, and Δn becomes positive for energies well above E_g.

2.1.2 Band-gap renormalization

A consequence of the Coulomb interaction among the photo-excited electronic excitations is the effect of the bandgap skrinkage (bandgap renormalization); i.e., the energies of the electrons and holes in their respective bands are reduced. This energy reduction is a consequence of the exchange effect for particles with equal spin, and Coulomb correlation effect for all particles. The exchange effect is caused by the Pauli exclusive principle. The probability that two Fermions with identical quantum numbers are at the same point in real space is zero. For increasing separation between the particles, the probability slowly approaches unity. Hence, the Pauli exclusion leads to a reduction of the probability that equally charged particles come close to each other, and this in turn reduces the repulsive (i.e., positive Coulomb energy) contribution.

An expression for the band-gap renormalization, originally derived by Wolff, is

$$\Delta E_g = -(\frac{e}{2\pi\varepsilon_0\varepsilon_s})(\frac{3n_{eh}}{\pi})^{1/3}, \tag{2.6}$$

where n_{eh} is the concentration of free electrons or holes, ε_0 is the permittivity of free space, and ε_s is the relative static dielectric constant of the semiconductor. The estimated shrinkage is proportional to the cube-root of the carrier concentration or the average interparticle spacing. We modeled the bandgap renormalization to cause a rigid translation (red shift) of the absorption curve. The change in absorption due to bandgap renormalization is predicted to be

$$\Delta\alpha(n_{eh}, E) = \frac{C}{E}\sqrt{E - E_g - \Delta E_g(n_{eh})} - \frac{C}{E}\sqrt{E - E_g}\,. \tag{2.7}$$

It predicts Δα, which is always positive, the largest near the bandgap and rapidly decreasing for higher energy. As with band filling, the change in refractive index was calculated by applying the Kramers-Kronig integral to Δα from bandgap renormalization, the largest change in refractive index is near the bandgap. Unlike band filling, however, the bandgap renormalization causes negative change in refractive index ($\Delta n < 0$) for energies above the bandgap as a result of decreasing in absorption coefficient for a fixed incident photon energy.

2.2 Temporal evolution in semiconductors

In semiconductors, the energy loss mechanisms of carriers play an important role in determining the carrier transport properties. When a semiconductor is in a thermodynamic equilibrium by excitation with optical sources, it reveals the non-equilibrium carrier distribution. The carrier energy after removal of excitation, in turn, is transferred first to the carriers and then to the lattice through several scattering processes. Various dynamical processes with characteristic time scales as shown in Fig. 2-1 can be divided into four temporally overlapping regimes in time domain sequence [37, 38]:

(a) Coherent regime. Initially, the photo-excited carriers have well-defined phase relationship with each other and with electromagnetic field that created the excitations. The coherence gradually vanishes and the momentum reorients (or randomize) by scattering events such as carrier-carrier scattering. For semiconductor, this time scale is often within a few tens femtoseconds.

(b) Non-thermal regime. The carriers behave quasi-classically and incoherently**.** The distribution of carriers after the destruction of coherence through dephasing is very likely to be non-thermal, and the distribution function cannot be characterized by a temperature. The energy distribution of the carriers will toward a Fermi-Dirac distribution with a defined temperature.

(c) Hot carrier regime. As thermalized carriers can be characterized by effective temperature T_c that still different from lattice temperature T_L, the carriers or called the hot carriers will be thermalized with lattice system through carrier and phonon interaction.

(d) Isothermal regime. All the carriers, phonons and exitons, are in equilibrium with each other can be described by one common temperature T_c. All the system will then return to thermodynamic equilibrium through carrier recombination (radiative or nonradiative) and diffusion. This time scale is on the order of > 100 ps.

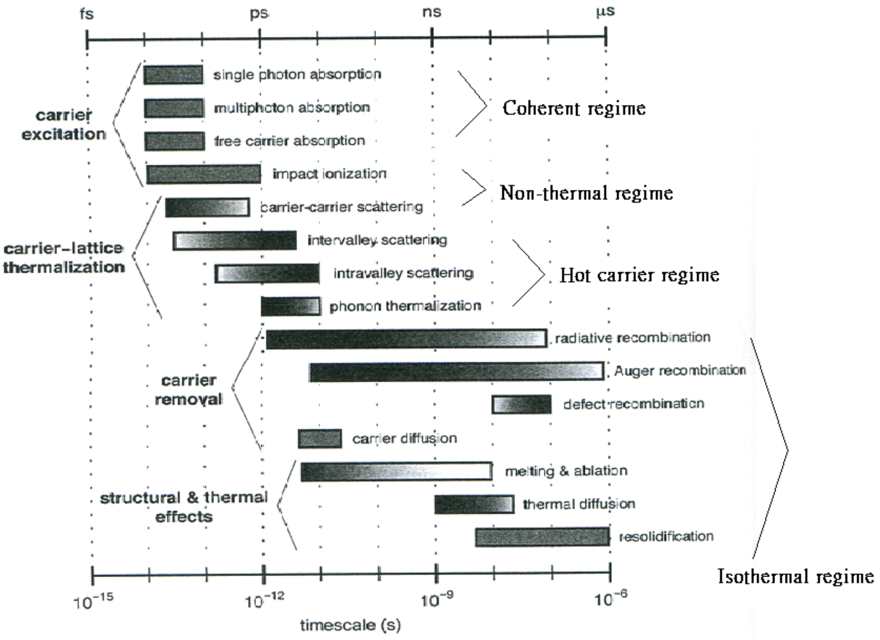

Fig. 2-1. Temporal evolution for various dynamical processes in semiconductors. [37]

2.3 Ultrafast physical processes

The dynamics of electrons, holes, excitons and phonons is influenced by their interaction with one another, as well as with defects and interfaces of the system. A free electron hole pair can be formed by absorbing the photon energy larger than the fundamental band-gap followed by the subsequent relaxation process via optical phonon emission as shown in Fig. 2-2. During the relaxation processes, electrons and holes undergo spatial and temporal evolution to achieve their quasi-equilibrium. In the following section, we focus on the mechanisms of carrier-carrier scattering and carrier-phonon scattering.

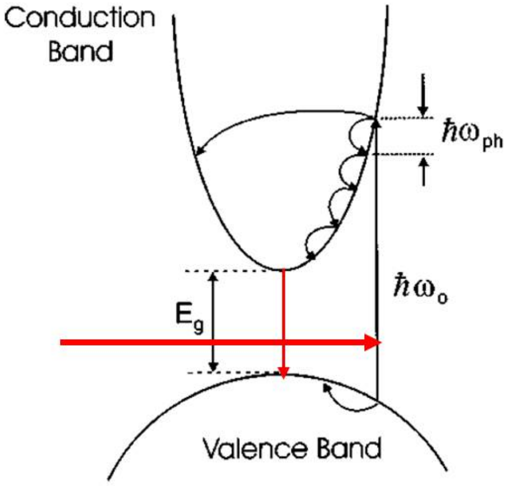

Fig. 2-2. The creation of electron-hole pair with optical excitation. Energy relaxation proceeds via phonon emission.

Carrier-carrier scattering determines the exchange of energy between carriers, and is responsible for the thermalization of excited non-thermal carriers. This process, including the electron-electron scattering, electron-hole scattering and hole-hole scattering, is a two-body collision and mediated by Coulomb interaction. It does not change the total energy and the number of carriers. The difference in the masses between electrons and holes reduces the energy between these two species. By using the Fermi golden rule of time dependent perturbation theory, the carrier-carrier scattering rate can be estimated. In addition, the exchanges of energy involved in carrier-carrier scattering should be greater than the energy changes in carrier-phonon scattering. The carrier-carrier scattering rate should be greater than the carrier-phonon scattering rate.

Carrier-phonon scattering plays an important role in the exchange of energy and momentum between carriers and the lattice. Optical phonon scattering and inter-valley scattering are the most frequent of all the carrier and phonon scattering events, which proceed with time scale on the order of 1 ps. In polar semiconductor, the longitudinal optical (LO) phonon emission rate [39], depending on the carrier energy and carrier density, is very large. At low temperature, carrier-phonon scattering is dominated by acoustic phonons interaction via deformation potential and piezoelectric field [40]. On the other hand, polar optical phonon scattering dominates at higher temperature.

2.4 Ultrafast measurement technique

Figure 2-3 shows the schematic diagram of the typical pump-probe measurement system. The incident ultra-short laser pulse is divided into to two pulse trains. The pump pulse is more intense of the two and the probe pulse is much weaker in order to produce the minimum disturbance in the sample. The separated beams follow different optical paths with one having a variable path length and varying the optical path length will in effect vary the time delay between the pump and probe pulses. The delay is typically done with a precise motorized transitional stage due to the extreme accurate requirements for temporal resolution. The two beams are then focused with spatially overlapping onto the sample. The intense pump beam induces change of absorption coefficient of sample and then the change of refractive index of sample can be calculated by applying the Kramers-Kronig relation [12, 41]. Besides, the probe beam carrying the information of changes produced by the pump is eventually detected with a photo-detector. So this time-resolved pump-probe measurement can be utilized not only for transmission properties but also for reflectivity investigation when recording the reflected optical probe signal.

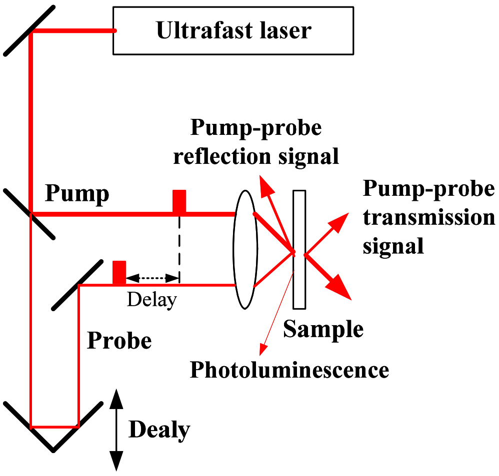

Fig. 2-3. Schematic of typical optical pump-probe measurement system.

2.5 Review of time-resolved studies in ZnO

2.5.1 Femtosecond time-resolved PL

To study time-resolved PL in femtosecond temporal resolution, Takeda et al. [42] have used optical Kerr gate (OKG) method for ZnO thin films. The experimental setup of OKG is shown in Fig. 2-4.

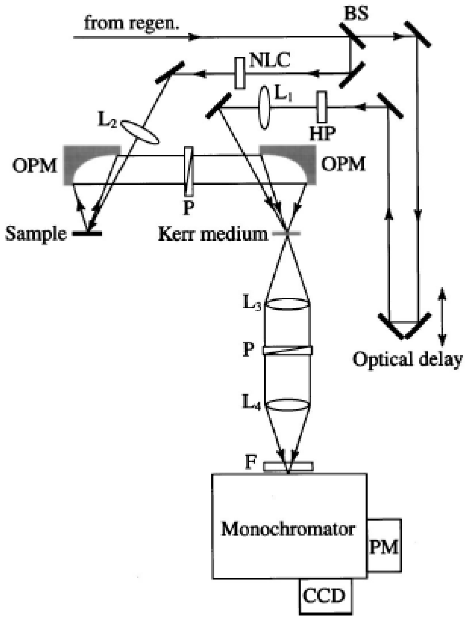

Fig. 2-4. Experimental setup for the optical Kerr gate (OKG) method. NLC: nonlinear crystal using a type-I BBO. [42]

Takeda et al. [33] have reported the time-resolved photoluminescence (TRPL) spectra with different delay time in a ZnO thin film as shown in Fig. 2-5. Besides, the time-integrated photoluminescence (TIPL) was depicted in the left top of Fig. 2-5. The emission peak from the electron-hole plasma (EHP) band can be observed with photon energy at 3.1 eV. The intensity of TIPL increases super-linearly with increasing the excitation intensity, which indicates that the EHP band is resulted from stimulated emission.

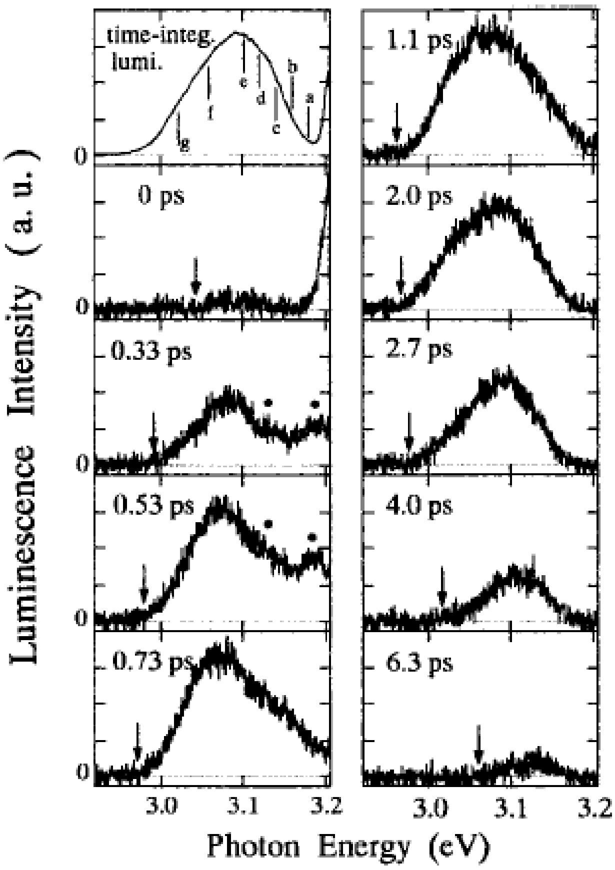

Fig. 2-5. Room temperature time-resolved photoluminescence spectra with different delay time in a ZnO thin film. [33]

The TRPL spectra show the buildup of EHP band from the initial signal of the pumping pulse partially via additional two PL peaks located at higher energy side as denoted by solid circles. The energy intervals from the pump pulse to the higher additional peak, and the higher peak to the lower one are almost the same with the value around 70 meV. The PL spectra show a red shift accompanied with the buildup of EHP band due to the band-gap renormalization (BGR). After time delay of 1 ps, the PL spectra reveal a blue shift due to the recovery of renormalized band-gap through the decrease of EHP emission.

2.5.2 Femtosecond transient absorption measurement

Under high excitation fluence of 90 μJ/cm^2, Yamamoto et al. [31] observed the transient optical gain spectrum in a ZnO epitaxial thin film by using the non-degenerate pump-prove technique. The measured result is shown in the Fig. 2-6 and the upper cure represents the absorption spectrum without pumping fluence. Free excitons A and B are considered overlapping at RT with the photon energy at 3.30 eV. The higher energy absorption peak observed at 3.395 eV is due to the LO-phonon and exciton scattering. The differential absorption was defined as ΔOD = OD (with pumping) – OD (without pumping).

There are three structures in the observed differential absorption spectra: (I) Decrease of the optical density around 3.330 eV, (II) increase of absorption at the lower energy side of the exciton absorption peak around 3.272 eV, and (III) negative absorption at the lower energy side around 3.22 eV. The structure (I) is related to the saturation of exciton absorption, while the structure (II) is concerned with the band-gap renormalization. And the optical gain due to the emergence of electron–hole plasma results in the structure (III).

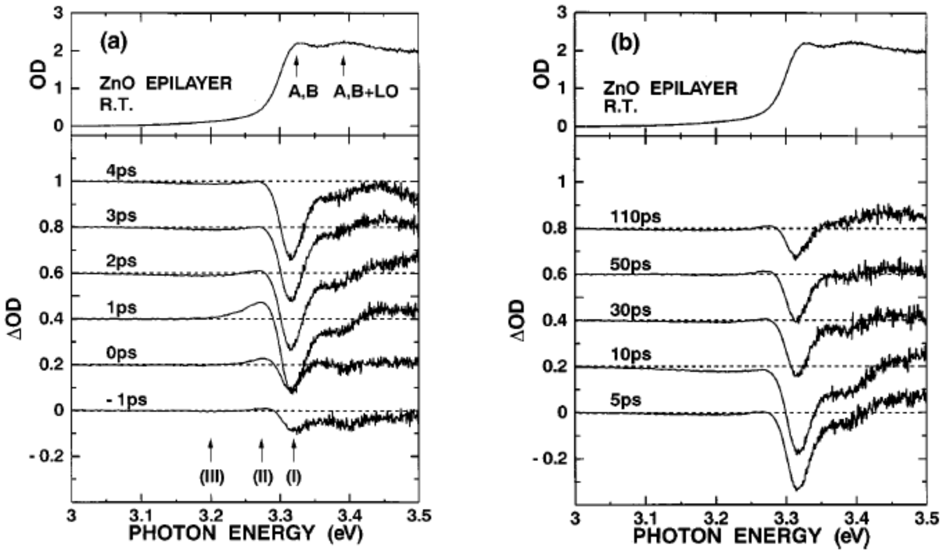

Fig. 2-6. The uppermost curve shows an absorption spectrum without pumping. Differential absorption spectra at various delay times are shown in the rest curves. Photon energies of the three structures (I), (II), and (III) are shown by the arrows. [31]

Although Takeda et al. have reported the transient EHP emission in ZnO by using the optical Kerr gate and Yamamoto et al. have observed the exciton absorption saturation and optical gain in ZnO by using the transient absorption measurements, the ultrafast thermalization for above band-gap states in a ZnO epitaxial thin film is still unclear. Besides, most TRPL studies focus on lasing dynamics and free exciton recombination in ZnO.

Hence, in order to directly observe the ultrafast thermalization for above band-gap states and realize the temporal evolution about free carriers convert into excitons, we investigated the carrier dynamics in a ZnO epitaxial film using the degenerate pump-probe at room temperature in Chapter 4. We also performed the dynamics in a thin (70-nm) and a thick (1-μm) ZnO epitaxial films to discuss the thickness effect on ultrafast thermalization of free carriers in above band-gap states. Also by using the pump-probe technique, we demonstrated the ultrafast free exciton relaxation with pumping dependence under resonant excitation in Chapter 5.

Chapter 3 Experimental setups

A variety of experimental methods have been employed to investigate the physical mechanisms, such as linear optical properties, PL characteristics and transient absorption phenomena. In this chapter, we first introduce the preparation of the used samples. Then, we used a commercial instrument to measure the absorption spectrum and carried out the time-integrated PL system with pulsed laser excitation. Finally, the complete setup of optically degenerate pump-probe technique was introduced.

3.1 Sample preparation

Our c-axis-oriented ZnO thin films with thickness of 70-nm and 1-µm were grown on the c-plane sapphire substrates by pulsed laser deposition with base vacuum of 2.1×10^{-8} torrs and working pressure of 1.1×10^{-7} torrs using a KrF excimer laser for different deposition times. Hall measurements yielded a background electron concentration of 1.68×10^{18} cm^{-3} for the 70-nm epifilm and 1.87×10^{17} cm^{-3} for the 1-µm epifilm, respectively. The detail growth apparatus and condition can be found in Ref. 43.

Our c-axis oriented ZnO/$Zn_{0.95}Mg_{0.05}O$ multiple quantum well structures (MQWs) was grown on a c-plane sapphire substrate using high-vacuum pulsed laser deposition (PLD) with KrF excimer laser. A ZnMgO buffer layer with thickness of 80 nm was deposited at 600 °C and subsequently annealed at 700 °C. The used MQWs comprised of five periods of $Zn_{0.95}Mg_{0.05}O$ barrier layers and ZnO quantum well layers. From the TEM measurement as shown in Fig. 3-1, the well layer thickness was around 8-39 nm, and the thickness of barrier layer was approximately 115 nm.

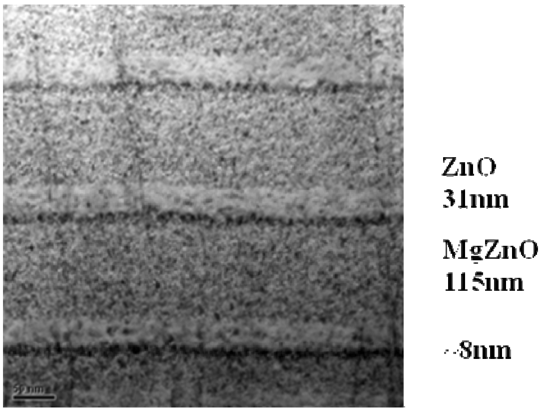

Fig. 3-1. The TEM measurement in ZnO/ZnMgO MQWs.

3.2 Measurement for absorption and time-integrated PL spectra

The absorption spectrum was measured at room temperature (RT) by using the spectral photometer (Jasco V-670) with resolution of 0.5 nm. In addition, the time-integrated PL (TIPL) excited by a frequency doubled mode-locked Ti:sapphire laser with central wavelength of 360 nm was recorded by a single grating monochoromator (iHR320) at RT. The TIPL system setup was shown in Fig. 3-2.

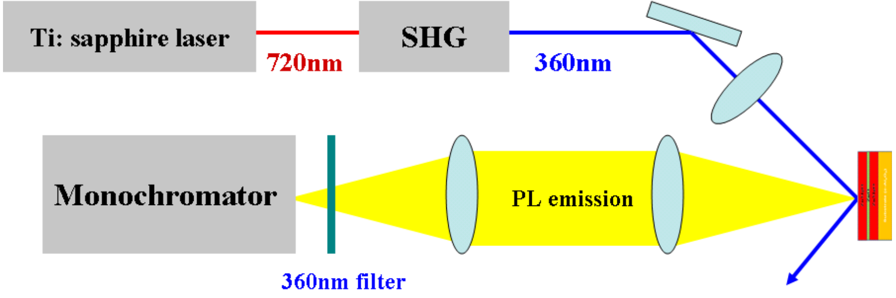

Fig. 3-2. System setup of time-integrated photoluminescence (TIPL) at RT.

3.3 Optical pump-probe system

The time-resolved optical pump-probe measurements as shown in Fig. 3-3 were also carried out at RT by utilizing a mode-locked Ti:sapphire laser (Tsunami, Spectral Physics Inc.) with 82 MHz repetition rate. The pulsed laser was equipped with a frequency doubler (Model 3980) to provide the ultraviolet (UV) excitation wavelength ranging from 360 nm (3.444 eV) to 383 nm (3.238 eV) with pulse width around 150 fs. The UV beam was divided by a beam splitter into a pump beam and a probe beam with intensity ratio larger than 20:1. The probe beam passed through a motorized translation stage in order to control the time delay relative to the pump one. The pump and the probe beams were focused and overlapped onto the sample surface by a focal lens with focal length of 5 cm. These two beams made a small angle and the beam diameter of pump beam is slightly larger than that of probe beam. Due to large absorption coefficient of 2×10^5 cm^{-1} near the band-edge, the transmitted light is too weak to be detected when the sample is thicker than 500 nm; and the reflection type measurement is required. The setup of time-resolved reflection is similar to the previous experimental arrangements [44].

For the purpose of reducing the coherent artifact, resulting from two beams interference if they possess the same polarization as well as distinguish-ability in detection, we kept the polarization of pump and the probe beams orthogonal to each other. Because our c-axis oriented ZnO epitaxial films were grown on the c-plane sapphire substrate, its crystal axis is normal to the surface. The probe beam incident normally to the sample surface has polarization orthogonal to the c-axis. Although there is a small angle (~ 8°) made between the pump beam and the surface normal, the pump beam with TE polarization is also orthogonal to the c-axis. The time-resolved setup in this work is independent of polarization. In order to increase the signal-to-noise ratio, the pump beam was modulated at 1 kHz by a mechanical chopper, and the transmitted probe beam was detected by a photo-diode and measured as a function of time delay by a lock-in amplifier.

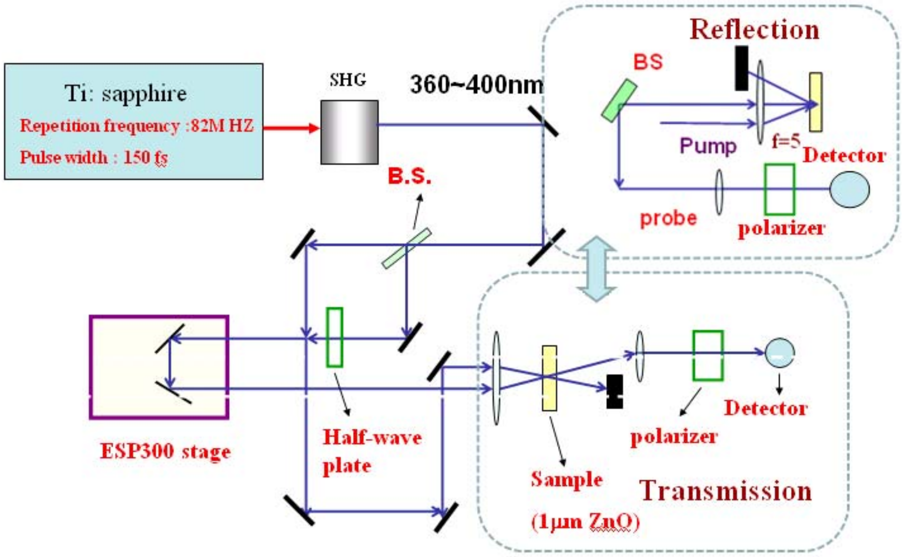

Fig. 3-3. Schematic diagrams of transmission and reflection type optical pump-probe measurement techniques.

3.4 Open-aperture Z-scan method

Z-scan is the most popular method due to its high sensitivity, simple experimental setup, and easy alignment [45]. We applied this method in our optical nonlinear absorption measurements.

The nonlinear absorption experiment as shown in Fig. 3-4 was demonstrated by using the standard on-axis open aperture Z-scan technique at RT. The laser pulse was modulated by a mechanical chopper, and then it was divided into the reflected and the transmitted beams by using a beam splitter. The reflected beam was measured by a photo-diode as the reference representing the incident light. The transmitted light was detected by another photo-diode and focused into the sample by a focal lens with focal length of 5 cm. The sample was mounted on a motorized translation stage controlled by the computer and moved along the z-axis with respect to the focus of the lenses. The output signals from these two photo-diodes were connected to a lock-in amplifier to increase the signal-to-noise ratio.

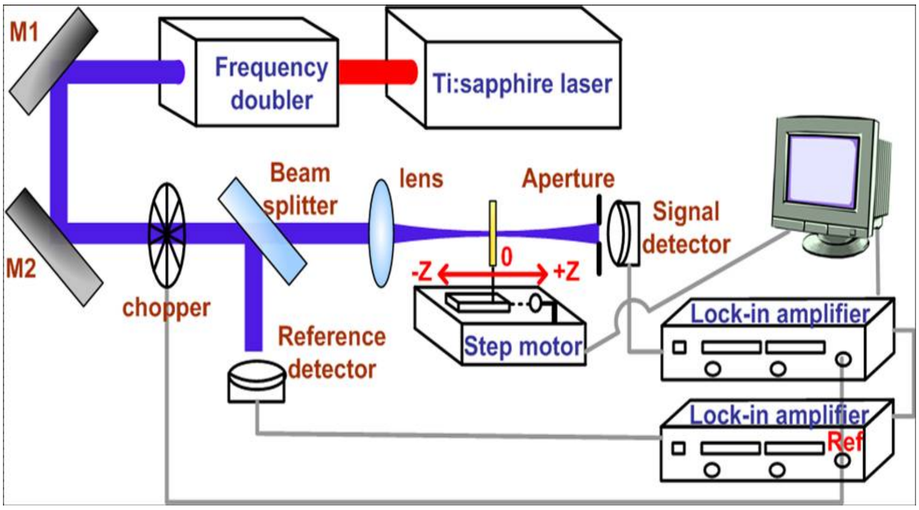

Fig. 3-4. The experimental arrangement for open-aperture Z-scan method.

Chapter 4 Thickness effect on ultrafast thermalization of free carriers in above band-gap states in ZnO epifilms

It is imperative to understand the thickness effect on free carrier thermalization in ZnO epifilms since they play important roles in stimulated emission and gain process in real photonic device structures. In this chapter, we investigate the intra-band relaxation via carrier-phonon scattering against the interaction between the free carriers and the sample surface by exciting the free carriers to the above band-gap states of two extreme thicknesses of epitaxial films at room temperature. In the following section, we compared free carrier dynamics in a thick (1-µm) and a thin (70-nm) ZnO epitaxial films with excited photon energy above the band-gap. It can be found that the loss of excited carrier density due to the surface trapping effect in the 70 nm epifilm can cause the energy dependent recovery time of renormalized band-gap; while the surface trapping effect can be neglected in the 1-µm epifilm. Therefore, it is useful to directly monitor the ultrafast thermalization and realize the temporal evolution of free carriers convert into free excitons from the analysis of carrier dynamics in the 1-µm ZnO epifilm by utilizing the reflection pump-probe.

4.1 Absorption and time-integrated PL spectra at RT

(a) 1-µm ZnO epifilm

Figure 4-1 shows the measured absorption spectrum and time-integrated (TI) PL spectrum of the c-plane ZnO epitaxial film with thickness of 1-µm grown on sapphire substrate at room temperature (RT). It reveals an absorption spectral edge at 376.5 nm or 3.293 eV corresponding to the free exciton transition. Considering the exciton binding energy of 60 meV, the band-gap energy (E_g) is around 3.353 eV or 369.7 nm. The linear absorption coefficient near the band-edge is around 2×10^5 cm^{-1}. Under inter-band excitation at RT, the TIPL spectra reveal a peak of 378 nm or 3.280 eV corresponding to excitonic spontaneous emission with FWHM of 98 meV. Due to large exciton and LO-phonon coupling, the LO-phonon replica can be observed on the low energy shoulder. The inset shows the TIPL spectrum with a longer wavelength scale indicating a high contrast ratio of UV to defect emission.

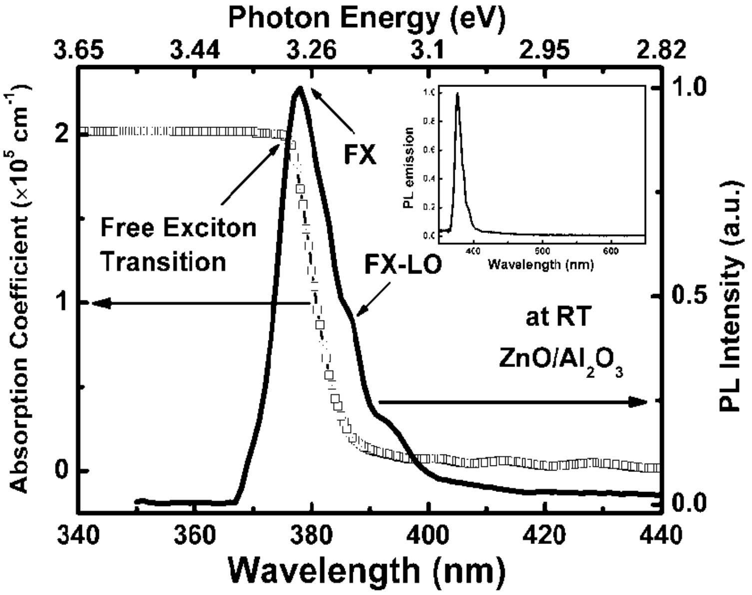

Fig. 4-1. Room temperature absorption spectrum (hollow squares) and time-integrated PL spectra (solid line) of a 1 μm ZnO epitaxial film. Inset: Time-integrated PL with a longer wavelength scale.

(b) 70-nm ZnO epifilm

Figure 4-2 shows the absorption and time-integrated photoluminescence (TIPL) spectrum of the 70 nm ZnO epitaxial layer at RT. We determined the free exciton transition from the absorption edge in Fig. 4-2 around 372 nm (3.333 eV), and estimated the band-gap energy to be around 3.393 eV by considering the exciton binding energy of 60 meV at RT. The linear absorption coefficient of free exciton transition is estimated to be around 2.2×10^5 cm^{-1}, also comparable to the value measured in ZnO single crystals [46]. The TIPL spectrum at RT under 1 and 10 μJ/cm^2 excitation reveals the emission peak around 376 nm (3.298 eV) corresponding to free exciton transition with FWHM of 102 meV. It is comparable to previous result [31], in which the peak position of PL spectra is located at 3.299 eV due to free exciton radiation at RT. It is also consistent with the result in Fig. 3 of Ref. [47], in which the PL peak is around 3.3 eV at RT. Due to large exciton-LO-phonon coupling in ZnO [48], several peaks on the lower energy shoulder are the LO-phonon replica. The excitation carrier density is determined by $N_{exc} = \frac{I_{exc}\alpha}{\hbar\omega_{exc}}$, where I_{exc} is energy flux density (or pump fluence) and $\hbar\omega_{exc}$ is photon energy. The focused diameter of pump and probe beams were measured to be 42-45 μm. We obtained the carrier density $N_{exc} \sim 2.32\times10^{18}$ cm^{-3} with I_{exc}=10 μJ/cm^2. Because the used sample is only 70 nm thick, the surface trapping will decrease the excited carrier density which the calculated carrier density directly from photo-excitation may be overestimated. We also normalized the measured TIPL spectra under 1, 10 and 20 μJ/cm^2 excitation, and found they are almost the same except for slightly increasing around the dip, about 43 meV below FX transition. It may be due to the line width broadening induced by heating under high pumping or hidden of EHP luminescence under excitonic luminescence. Previous studies reported by Klingshirn et al. [47], have shown the electron-hole plasma (EHP) emission in the range from 3.34 eV to 3.28 eV at 10K, shifting with increasing excitation density.

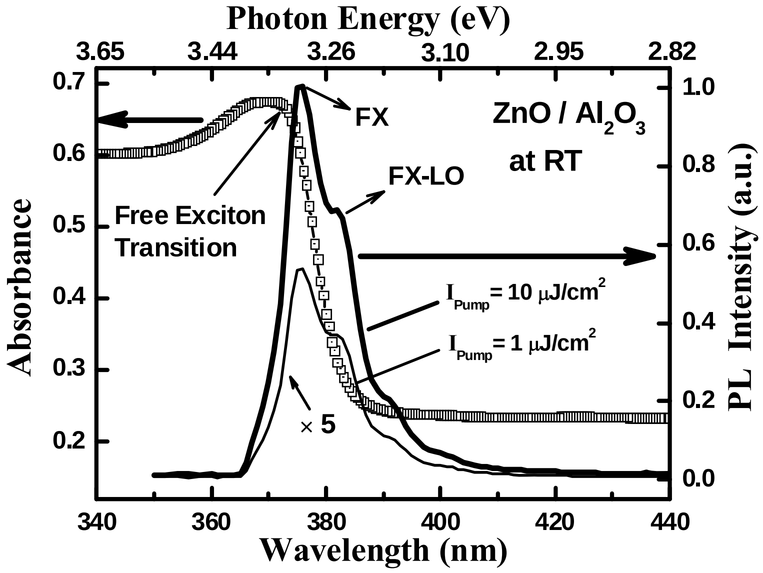

Fig. 4-2. Absorption spectrum (hollow squares) and TIPL spectra (solid lines) with excitation of 1 μJ/cm^2 (thin line) and 10 μJ/cm^2 (thick line) in a 70 nm ZnO epitaxial layer at RT.

(c) ZnO/ZnMgO MQWs

Figure 4-3 shows the RT absorption and the time-integrated PL (TIPL) spectra of ZnO/$Zn_{0.95}Mg_{0.05}O$ multiple quantum well structures (MQWs) grown on c-plane sapphire. The absorption spectrum reveals an absorption spectral edge around 373 nm or 3.324 eV corresponding to the free exciton transition of ZnO QWs, and another one around 345 nm or 3.594 eV corresponding to the near band-edge absorption of ZnMgO barrier. The TIPL spectra show emission peak around 377 nm or 3.289 eV corresponding to free exciton spontaneous emission with FWHM of 108 meV resulted from exciton-phonon scattering. The PL peak shows a Stokes shift of 35 meV and is located on the lower energy side of free exciton absorption band.

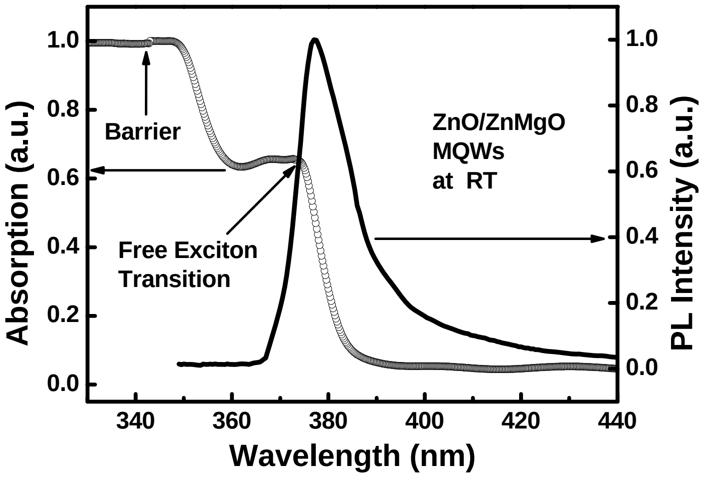

Fig. 4-3. Room temperature absorption spectrum (hollow circles) and time-integrated PL spectra (solid line) in ZnO/ZnMgO multiple quantum wells.

From the absorption and TIPL measurements above, we compared the band-gap energy, PL emission peak, full-width half maximum, and Stokes shift of three samples as shown in the table 4-1. It can be found the linear optical properties in ZnO/ZnMgO behave like a thin epifilm and the quantum confinement effect cannot be observed.

	1-µm	70-nm	MQWs
E_g (eV)	3.353	3.393	3.384
Emission Peak (eV)	3.280	3.298	3.289
FWHM (meV)	98	102	108
Stokes shift	13	35	35

Table 4-1. Comparison of Eg, emission peak, FWHM, and Stokes shift in three samples.

4.2 Free carrier dynamics in the 1-μm ZnO epifilm

4.2.1 Measurement of transient reflectance

The transient normalized differential reflectance (ΔR/R) as a function of time delay for excitation photon energy above the band-gap at 3.444, 3.425, 3.388 and 3.369 eV were shown in Fig. 4-4. First, around zero time delay we found a negative dip resulting from two-photon absorption (TPA) of simultaneously absorbing one pump and one probe photon. After the TPA, a peak appears due to initially excited free carriers by the pump pulse and then quickly decreases to negative differential reflectance. The negative transient differential reflectance slowly reduces to the original ΔR = 0 level and then transits to a positive one. Finally, there is a relatively slow decay at the long time delay. It can be seen that these four traces are similar except that the peak amplitude decreases with decreasing the photon energy.

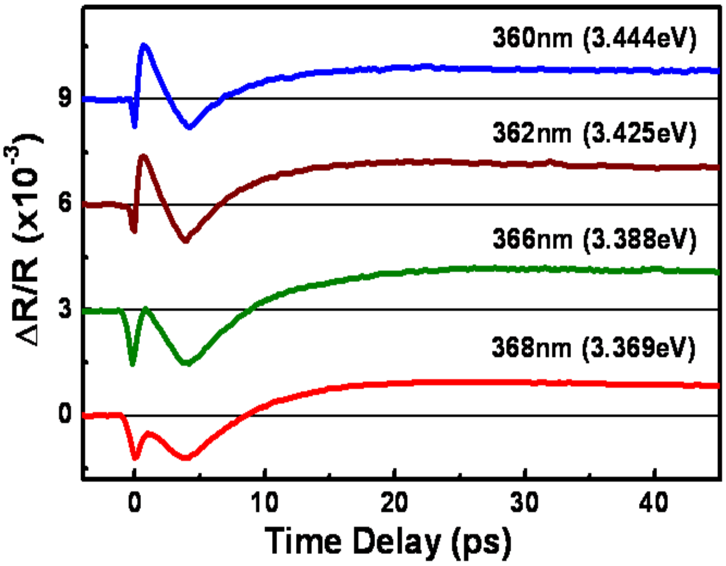

Fig. 4-4. Measurement of transient normalized differential reflectance as a function of time delay. For excitation photon energy at 3.444, 3.425, 3.388 and 3.369 eV. Traces are vertically displaced for clarity.

4.2.2 Energy dependent ultrafast thermalization

To analyze the measured temporal traces in Fig. 4-4, a decomposition fitting procedure is used to extract the phenomenological responses and their time constants after zero time delay by $a_1\exp(-t/\tau_1) - a_2\exp(-t/\tau_2) + a_3\exp(-t/\tau_3)$. The fitting results for excitation photon energy at 3.444 eV is shown in Fig. 4-5(a) and similar process can be done for the rests. We show the fitted time constants of τ_1 and τ_2 as a function of excitation photon energy in Fig. 4-5(b). In general, the generated hot carriers will be scattered away from their initial optically-excited states through either carrier-carrier scattering during coherent regime within a very short time scale less than 200 fs or external thermalization via carrier-phonon scattering to achieve quasi-equilibrium with the lattice system as described in Chapter 2. Then, the hot carriers release their excess kinetic energy through phonon emission and relax to the bottom of the conduction band. Because the pulse-width of used excitation laser is around 150 fs, we are not supposed to observe the carrier-carrier scattering. Thus, the obtained ultrafast decay time τ_1 around 1.0-1.5 ps is mainly due to the carrier-phonon scattering. This is comparable to previous studies of external thermalization in GaN [49] and InGaN [50]. As shown in Fig. 4-5(b), the performed decay time τ_1 slightly decreases with decreasing the photon energy. A strong hot phonon effect is expected in ZnO because of large LO-photon energy around 72 meV. As a consequence, the free carrier thermalization is affected by the assistance of optical-phonon for well above band-edge states; while it is mainly due to the assistance of acoustic-phonon for near band-edge states (excess energy < 26 meV).

The time constant τ_2 is on the order of 4.6-5.0 ps, it is interesting to compare the measured results with the previous time-resolved PL studies in ZnO thin films and nanostructures. Previous time-resolved PL reports showed a blue shift of PL emission with a time constant of 2.5 ps due to the recovery of the renormalized band-gap in ZnO thin films by using the optical Kerr gate method [33]. Takeda et al. [51] found that the P-band emission after a time delay of 4.5 ps accompanied with free carriers convert into free excitonic state under band-to-band excitation. Kwok et al. [52] measured the decay times of 7 ps and 10 ps in ZnO rods and shells, respectively, which most likely due to non-radiative decays. The obtained time constant τ_2 is almost independent of photon energy that means the recovery time is concerned with the decay rate of thermalized carriers with Fermi-Dirac distribution near the minimum of renormalized band-edge. Here, we attributed τ_2 to the recovery process of renormalized band-gap accompanied with the decrease of free carriers via non-radiative channel, such as multi-phonon emission, trapping by defects, Auger recombination and forming excitons. The measured third time constant τ_3 on the order of 90-100 ps, independent of the photon energy, is attributed to exciton and/or free carrier recombination.

In general, the excited free carriers will result in both the band-filling (BF) and the band-gap renormalization (BGR) effects in semiconductors [41]. The band-filling or known as the Burstein-Moss effect reduces the inter-band transition due to the Pauli exclusion principle; the BGR resulting from the exchange interaction among excited carriers reduces the single-particle potential energy to cause the shrinkage of band-gap. The temporal evolution results from the interplay between BF and BGR effects can be observed in this work. For excitation energy above the band-gap states as shown in Fig. 4-4, the BF and BGR effects emerge simultaneously by pulsed photo-excitation and compete to each other in determining the magnitude and sign of transient differential reflectance ($\Delta R/R$) at time delay of 0.67 ps. The minimal $\Delta R/R$ at time delay of 3.4 ps indicates the dominance of BGR effect. After the recovery of renormalized band-gap, the rest thermalized carriers occupy the bottom of conduction band or convert into free excitons, which the transient $\Delta R/R$ at time delay of 15 ps is attributed to the dominance of BF effect.

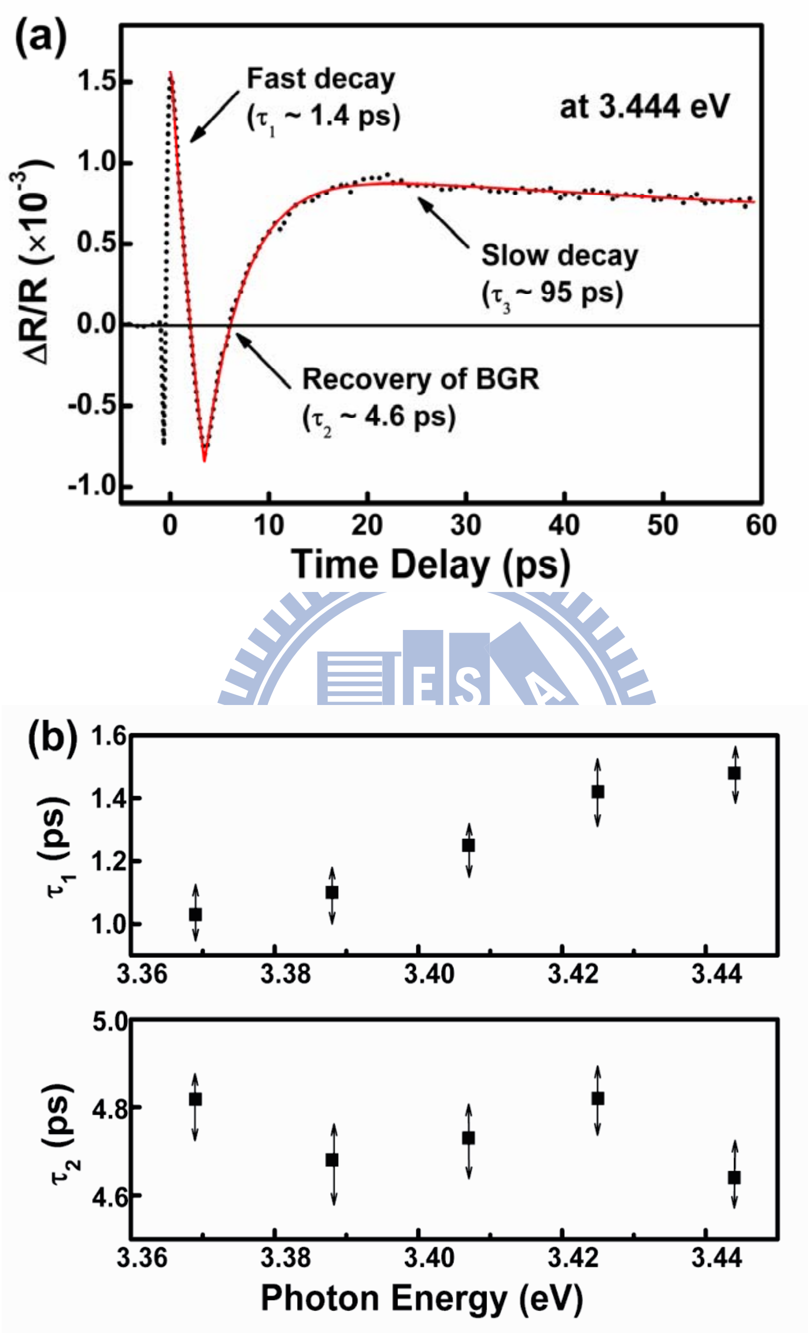

Fig. 4-5. (a) The measurement of time-resolved reflectance (dotted line) and the fitting curve (solid line) with their corresponding decay time constants for excitation photon energy at 3.444 eV. (b) The fitted first and second time constants as a function of photon energy. The arrows indicate the error bar.

4.3 Free carrier dynamics in the 70-nm ZnO epifilm

4.3.1 Well-above band-gap states

The normalized transient differential transmissions (ΔT/T) as a function of time delay for excited photon energies of 3.464 eV (358 nm) and 3.444 eV (360 nm), having excess energy of 71 and 51 meV above the conduction band edge (CBE), in a 70 nm film with E_g= 3.393 eV are shown in Fig. 4-6. Here, the difference in transmission, ΔT =T (with pump) – T (without pump), represents the change of transmission through the sample with and without optical pumping. It shows a negative dip resulting from two-photon-absorption (TPA) coinciding with the pump pulse. The transient response instantaneously increases to become positive after the pump pulse then gradually decreases to negative again. Finally, the negative transient response returns to the original level at long time delay. In general, the excited free carriers will result in both the Burstein-Moss effect, also called the band-filling effect, and the band-gap renormalization (BGR) effect in semiconductors [41]. Here, the measured transient differential transmission, varying from positive (induced transmission) to negative (induced absorption), reflects that the Burstein-Moss effect is diminished by the BGR effect with the excited carriers quickly relaxing to the conduction band edge (CBE). The transient differential transmission at 3.444 eV is similar to that at 3.464 eV, except that it decays slightly faster to result in earlier transition to negative differential transmission.

In order to extract the free carrier relaxation times in the 70 nm ZnO film, we use the response function of $A_1\exp(-t/\tau_1)$ - $A_2\exp(-t/\tau_2)$ to fit the time traces in Fig. 4-6, where A_1 term is a fast exponential decay component due to the Burstein-Moss effect and A_2 term is a slow exponential decay component corresponding to the BGR recovery. A relaxation time (τ_1) of 14.5 and 9.8 ps is found for photon energy of 3.464 and 3.444 eV, respectively. The prolonged relaxation process is mainly due to the carrier-phonon scattering with their excess kinetic energy. Both times are longer than 1 ps observed in ZnO films using time-resolved PL techniques [33]. The recovery time for BGR (τ_2) of 22.5 and 15.3 ps corresponding to photon energy at 3.464 and 3.444 eV, respectively, is close to the non-radiative recombination time on the order of 10 ps reported in ZnO nanorods [32].

From the measurements of far-above band-gap dynamics, we notice two cases worthwhile to be discussed. First, the far-above band-gap dynamics reveals a long-time relaxation as compared with previous reports [32, 33]. Second, an even longer carrier relaxation was observed for excitation to higher lying states when using 3.464 eV than that at 3.444 eV. Because the thickness of sample used in the study is as thin as 70 nm, the interaction between excited free carriers and surface of the thin film may play a role in the relaxation process. We therefore estimate the time elapsed for a free carrier to travel a distance of 70 nm by the equation: $t = \frac{d}{\sqrt{2E_k / m_c^*}}$, where d represents the thickness (70 nm) of sample and $m^*_c = 0.28\ m_0$ is the effective mass of electrons. For the excess energy (E_k) of 71 meV and 51 meV provided respectively by the 3.464 eV and 3.444 eV photons, we obtained time constants around 235 fs and 276 fs. This is close to the reported thermalization time of 200 fs for carrier-carrier or carrier-phonon scattering in ZnO [32]. The physical picture is an excited free carrier may impinge on surface of the sample prior to interaction with phonons or other carriers to lose their excess kinetic energy. Thus, we attribute the long intra-band relaxation of the carriers toward the band-edge to inefficient thermalization for carrier-phonon scattering after the carriers scattered by the sample surface. Furthermore, some excited free carriers might have been trapped by the surface when they impinge on it. It is known, the BGR effect is concerned about exciting enough free carriers to result in shrinkage of the band-gap due to screening of Coulomb interaction [41]. The BGR effect will produce negative differential transmission to the transient response with photo-excitation above the band-gap states [32]. Both the loss of free carrier density via surface trapping and fast carrier escape from the region of measurement could result in the decrease in the BGR effect e.g., the higher the excess energy, the more probable the loss of carrier density which causes the weaker BGR effect, and thus longer recovery time for the higher excitation photon energy.

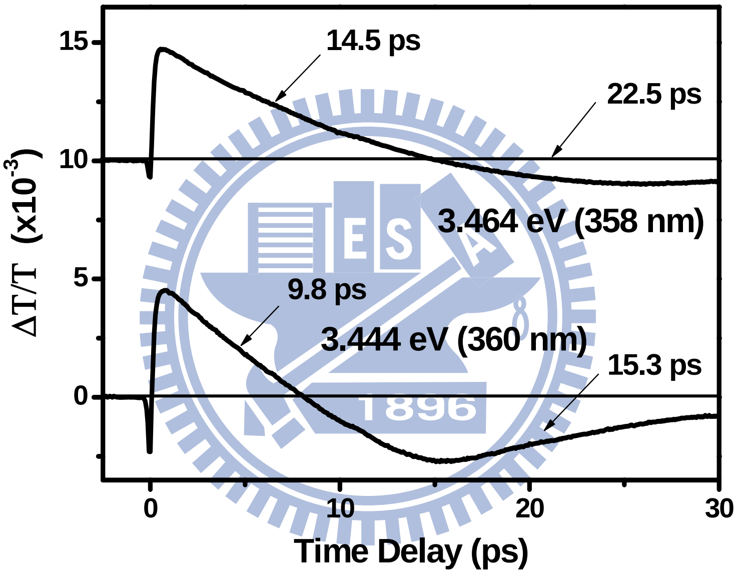

Fig. 4-6. Measurement of normalized transient differential transmission as a function of time delay for excitation photon energy at 3.464 and 3.444 eV in the 70 nm ZnO epifilm. Traces are vertically displaced for clarity.

To confirm that the loss of excited free carriers plays an essential role in the onset of BGR effect, we compared the same carrier dynamics analysis for the 1 μm ZnO epifilm with E_g=3.353 eV under the same optical excitation. The measured normalized transient differential reflectance for photon energy ranging from 3.444 eV to 3.369 eV is corresponding to the excess energy ranging from 91 meV to 16 meV in the conduction band as shown in Fig. 4-4. As compared with the measurements in the 70 nm epifilm as shown in Fig. 4-6, the dynamics in the 1 μm epifilm reveals an ultrafast relaxation, implying the carrier thermalization due to carrier-phonon scattering in the thick epifilm is more efficient than in the thin epifilm. It can be found that the free carrier relaxation time is on the order of 1.0-1.4 ps in the 1 μm epifilm, while it takes much longer time (> 9 ps) with a dependence upon excitation photon energy in the 70 nm epifilm. These results indicate effective hot carrier thermalization via carrier-carrier or carrier-phonon scattering in the 1 μm epifilm, but inefficient hot carrier thermalization in the 70 nm epifilm. As a result, we found decrease in the BGR effect and the variation of BGR build-up time in the 70 nm epifilm.

4.3.2 Near-band-edge states

When we decrease the excitation photon energy toward the CBE, the measured normalized transient differential transmissions as a function of time delay for photon energy at 3.425 eV (362 nm) and 3.416 eV (363 nm) in the 70 nm film with E_g = 3.393 eV are shown in Fig. 4-7. The data show a negative dip due to TPA around zero time delay, and an obviously quick transition from positive transient response to negative followed by the slow recovery process of negative response. The relaxation observed for 3.425 eV excitation, which provides 32 meV excess energy, is much faster than those observed for 3.464 and 3.444 eV in Fig. 4-6, implying the carrier thermalization occurs instantaneously after the pump pulse and the interaction with the sample surface can be ignored. It can be anticipated that both of BF and BGR effects happen almost simultaneously. In addition, the efficient carrier thermalization results in an ultrafast decay and the BGR effect can produce negative differential transmission to the transient response, respectively. Thus, the recovery of BGR via free carrier recombination causes transferring to the Burstein-Moss effect and the negative transient response returns to positive at longer time delay.

As we further decrease photon energy to near the band-gap, the trace obtained for 3.416 eV excitation (23 meV above the CBE), also shown in Fig. 4-7, consists of a fast and a slow decay component. There is no negative transient response in this trace. The photo-generated carriers acquire the Fermi-Dirac distribution through carrier-carrier scattering, and then quickly relax to the band-edge through carrier-phonon scattering [53]. Under this circumstances, the downshift of band-gap by the BGR effect at RT may not be large enough to exceed to the width of thermalized carrier distribution (~ 26 meV) limited by the band-edge and the Burstein-Moss effect should be always present. Thus, the Burstein-Moss effect still overwhelms the BGR effect when performed the experiment near the band-edge. Furthermore, at relatively longer time delay, the carriers will decay through carrier recombination.

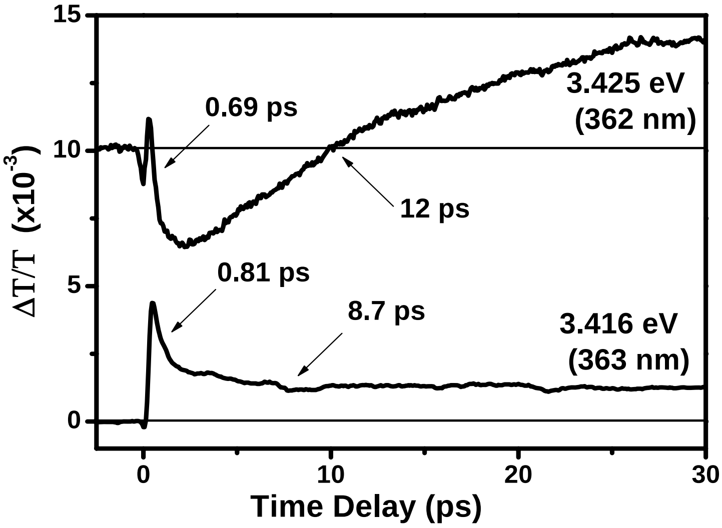

Fig. 4-7. Measurement of normalized transient differential transmission as a function of time delay with excitation photon energy at 3.425 and 3.416 eV in the 70 nm ZnO epifilm. Traces are vertically displaced for clarity.

By using the same fitting as described above to the trace for 3.425 eV excitation in Fig. 4-6, we obtained a fast decay time of 0.69 ps and a recovery time of 12 ps. In addition, we obtained fast and slow decay times of 0.81 and 8.7 ps (with positive sign of A_2) to the trace for 3.416 eV excitation. The fast decay times (0.69 and 0.81 ps) are consistent with the carrier thermalization time on the order less than 1 ps reported in ZnO thin films [31, 33]. Whereas, the BGR recovery time (12 ps) or the slow decay time (8.7 ps) obtained from this work is due to the non-radiative recombination also consistent with previous reports [32].

4.4 Summary

The energy dependent free carrier dynamics was investigated in the thin (70-nm) and the thick (1-μm) ZnO epifilms by using the optical pump-probe technique at RT. The measured result in the 1 μm ZnO epifilm shows that the ultrafast thermailization time increases as increasing the excitation photon energy accompanied with the hot phonon effect; while the recovery time of renormalized band-gap, associated with the non-radiative decay or the free exciton formation, is independent of photon energy. The far-above band-gap dynamics in the 70 nm epifilm reveals the prolonged relaxation time and the slow recovery of renormalized band-gap. Moreover, the band-gap renormalization (BGR) effect is affected by the inefficient carrier-phonon scattering, and the loss of excited carrier density via surface trapping results in an energy dependent BGR buildup time. However, the far-above band-gap dynamics in the 1 μm epifilm reveals fast relaxation followed by BGR recovery due to the surface trapping effect can be ignored. The near band-edge dynamics shows an ultrafast carrier thermalization both in the thin and the thick epifilms.

Chapter 5 Ultrafast free exciton relaxation with pumping dependence in ZnO epitaxial films

Transient absorption measurements have been commonly performed in GaN and related III-V materials on time scales of femtosecond to nanosecond. For example, from the non-degenerate nanosecond pump-probe technique, GaN thin films reveal large optical nonlinearities associated with exciton saturation. Yamamoto et al. have reported the optical gain on the lower energy side of free exciton state in ZnO thin films by measuring the transient absorption with band-to-band excitation. Though there were some time-resolved reports in ZnO, most TRPL studies focusd on lasing dynamics and free exciton recombination.

In this chapter, we observed the femtosecond resolved excitonic relaxation and absorption saturation by measuring the transient differential transmission in the 70-nm ZnO epitaxial layer at RT. The analysis of pumping dependent relaxation suggests the transition from exciton-phonon scattering into exciton-exciton scattering under an increase in pumping fluence. We also performed the ultrafast free exciton dynamics in the 1-μm ZnO sample by utilizing the reflection pump-probe at RT. Based on a theoretical model in calculating the change of refractive index (Δn) in ZnO, we analyze the measured spectral dependence of transient reflectance and demonstrate the significance of competition of band-filling (BF) and band-gap renormalization (BGR) effects.

5.1 Free exciton transient absorption in the 70-nm epifilm

5.1.1 Measurement of transient transmission

The normalized transient differential transmissions ($\Delta T/T$) near free exciton transition as a function of time delay for excitation wavelengths at 372 nm (3.333 eV) and 373 nm (3.324 eV) also with 10 μJ/cm^2 excitation are shown in Fig. 5-1. At the beginning of the pulse excitation, an instantaneous rise around zero time delay can be seen, and then the photo-generated carriers quickly quench the absorption to result in the band-filling effect. Generally speaking, the photo-excited free carriers are scattered out of their initial states through carrier-carrier interaction, which is comparable to the time scale around pulse duration, and then quickly relax to reach the quasi-equilibrium with the lattice system through carrier-phonon interaction. Thus, the decrease of transient differential transmission can be attributed to the free carriers consume their kinetic energy via carrier-carrier and carrier-phonon scattering. Because the excitonic states are simply occupied by the resonantly generated excitons, the absorption saturation by the band-filling (BF) can be achieved [31, 41, 54]. The absorption saturation due to the occupancy of non-equilibrium excitons is sufficient to produce decrease of absorption resulting in a measurable differential transmission even with spatially averaging over the probe beam profile, which is just slightly smaller than the pump one. The fast recovery of absorption saturation can be attributed to excitonic thermalization process through phonon emission. After the thermalization, the decrease in exciton population via either radiative or non-radiative recombination causes the slow recovery.

In order to extract the time constants of free carrier relaxation, the best fitting for the excitation at 372 and 373 nm in Fig. 5-1 were achieved in use of three decay times as: $A_1\exp(-t/\tau_1) + A_2\exp(-t/\tau_2) + A_3\exp(-t/\tau_3)$. An ultrafast time constant τ_1 of 0.82-0.85 ps can be obtained due to excitonic thermalization. According to previous TRPL studies of EHP dynamics in ZnO thin films by using the optical Kerr gate method [33], the red shift of PL emission was observed with a time constant less than 1 ps during the build-up stage of EHP state. Because the formation of EHP state is concerned about photo-excited enough carriers to achieve the Mott transition, the screening of Coulomb interaction and the band-gap renormalization effects need to be considered during the relaxation process. However, we pumped the sample here with lower excitation density and monitored the intrinsic non-equilibrium excitonic state. Thus, the reported ultrafast relaxation time of 0.82-0.85 ps is mainly due to the thermalization process through exciton-phonon or exciton-exciton scattering. Furthermore, the time constant τ_2 of 8.46-8.95 ps should be predominately caused by the non-radiative channels, such as trapping by defects, multi-phonon emission, or Auger recombination. And the time constant τ_3 of 47.8-53.2 ps is attributed to the longer radiative lifetime, which is comparable to the previous TRPL studies that the spontaneous recombination time is on the order of 46 to 110 ps in ZnO films grown by MBE and 30 to 74 ps in rf-sputtered films [22, 55].

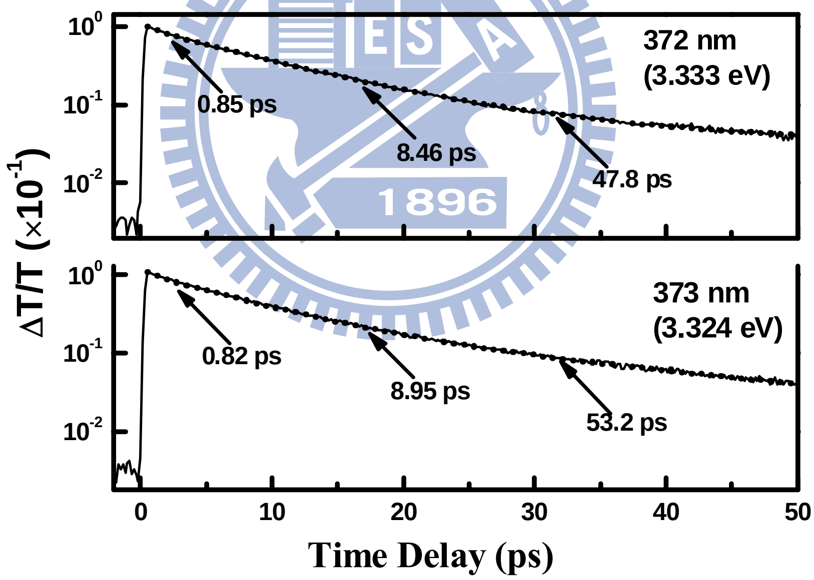

Fig. 5-1. Measured normalized transient differential transmission as a function of time delay for excited photon wavelength at 372 and 373 nm. Dotted lines are fitting curve.

5.1.2 Pumping dependent relaxation

In order to realize the mechanism of free exciton thermalization, we performed the pumping dependent dynamics and nonlinear absorption near exciton resonance. Figure 5-2 shows the free exciton dynamics for three different pumping densities. We found the ultrafast relaxation time on the order of 800-900 fs is almost independent of the pumping fluence under 1-20 μJ/cm^2. This ultrafast relaxation time is responsible for free exciton thermalization via exciton and phonon scattering. However, the relaxation time slightly decreases to 700-800 fs as increasing the pumping fluence to 30-50 μJ/cm^2. By using the optical Kerr gate measurements, previous TRPL studies reported the build-up of P-band emission with a time constant of 800 fs through exciton-exciton scattering in ZnO thin films [56]. Consequently, the decrease of relaxation time with increasing pumping fluence supports the transition of excitonic thermalization from exciton-phonon scattering at low pumping into exciton-exciton scattering at high pumping.

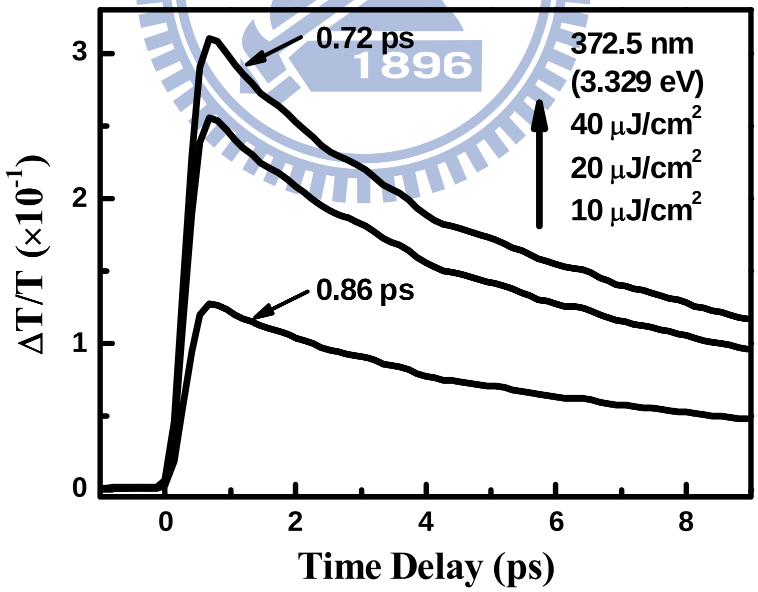

Fig. 5-2. Measured normalized transient differential transmission as a function of time delay for excited photon wavelength at 372.5 nm under pumping density of (from bottom to top) 10, 20 and 40 μJ/cm^2.

5.1.3 Transient absorption saturation at near exciton resonance

The maximal normalized differential transmission as a function of excitation energy from the above band-gap to the band-tail states was plotted in Fig. 5-3 The largest induced transparency due to absorption saturation occurs at 372.5 nm (3.329 eV), corresponding to the free exciton transition. It can be obviously observed that the maximum of △T/T near the free exciton transition (372.5 nm) is five-times larger than the value near the band-gap state (365 nm) in Fig. 5-3, although their linear absorption coefficients are almost the same. Under exciton-resonant excitation, the excited free excitons can be ionized to become free electrons through the assistance of optical phonon, which the free e-h pairs and free excitons coexist in this system. The access free electrons cause the screening of Coulomb attractive potential to introduce the so-called band gap renormalization (BGR). According to previous studies, the investigation of transient absorption in GaAs and ZnTe quantum wells at RT [57, 58], that the bleached exciton absorption by excited resonant excitons is stronger than the same density of free electron-hole pairs. Thus, we can mainly attribute the negative differential absorption to the band-filling of resonantly excited excitons, while the screening effect may play a minor role [57, 58]. Because the measured differential reflectivity (ΔR/R) is on the order of 10^{-3}, whereas the measured differential transmission (ΔT/T) is on the order of 10^{-1}, we neglected the change of reflectance and deduced the differential absorption from the differential transmission based on the equation of: $\Delta\alpha = -\frac{1}{d}\ln(1+\frac{\Delta T}{T})$ with d being the thickness of sample. The value of Δα is estimated to be -1.8×10^{4} cm^{-1} near exciton resonance under 10 $\mu\text{J/cm}^2$ excitation that is comparable to the results in GaN at 10K and in GaAs at 15K measured with the differential transmission spectrum (DTS) by using the pump-probe technique [28, 59].

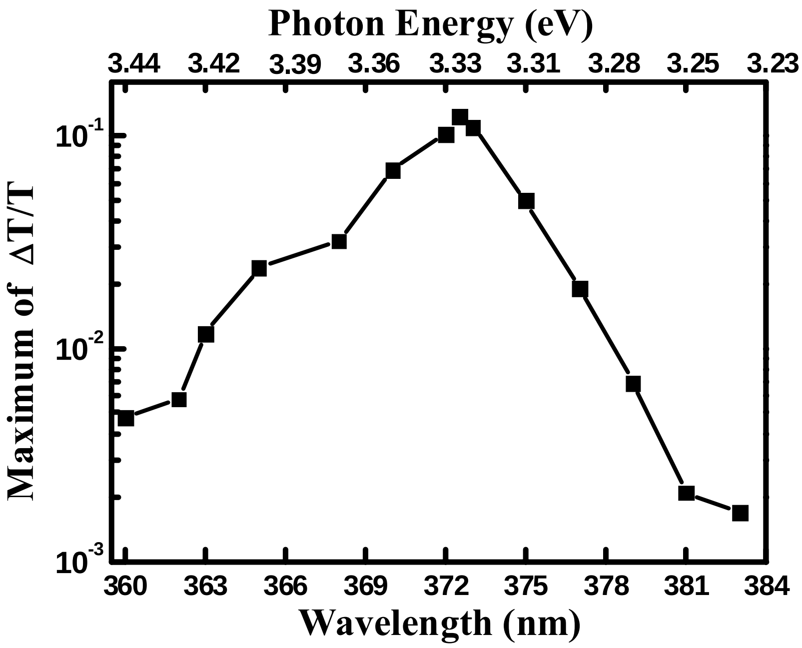

Fig. 5-3. The maximal differential transmission as a function of excitation wavelength under pumping fluence of 10 μJ/cm^2.

The negative differential absorption maximum as a function of pumping density is shown in Fig. 5-4 with fluctuation of pumping fluence about 0.2 μJ/cm^2. Because the temporal regime of the measured differential absorption on the order of pulse duration is shorter than the relaxation process, the negative differential absorption maximum is mainly due to the absorption saturation by band-filling effect. To estimate the saturation intensity, we fit the experimental results by using the absorption saturation model [60],

$$\left|\frac{\Delta\alpha}{\alpha_0}\right| = \frac{(1-x)(I/I_S)}{1+I/I_S}, \tag{5.1}$$

where $\Delta\alpha$ is the differential absorption maximum within the pulse duration, α_0 is the absorption coefficient without pumping, x is the non-saturated portion of absorption and I_S is the saturation intensity. We obtained $x = 0.65$ and $I_S = 25$ μJ/cm^2. It means that about 35% of resonantly excited excitons contribute to the band-filling. As pumping fluence up to 50 μJ/cm^2, a constant value of $\Delta\alpha \sim$ -4.7×10^4 cm^{-1} will be reached. In addition, the maximal differential absorption reveals a linear dependence of pumping fluence (< 20 μJ/cm^2) due to exciton-phonon scattering. The emergence of non-linearity as running off the linear dependence with pumping fluence around 20 μJ/cm^2 (corresponding to carrier density of 4.6×10^{18} cm^{-3}) as shown in Fig. 5-4. When performed larger than 20 μJ/cm^2 excitation, it reveals a nonlinear dependence of pumping fluence which indicates the saturation of band-filling due to exciton-exciton scattering or transition to an EHP. Similar results were reported in GaN thin films at 4 K under exciton resonant excitation [30].

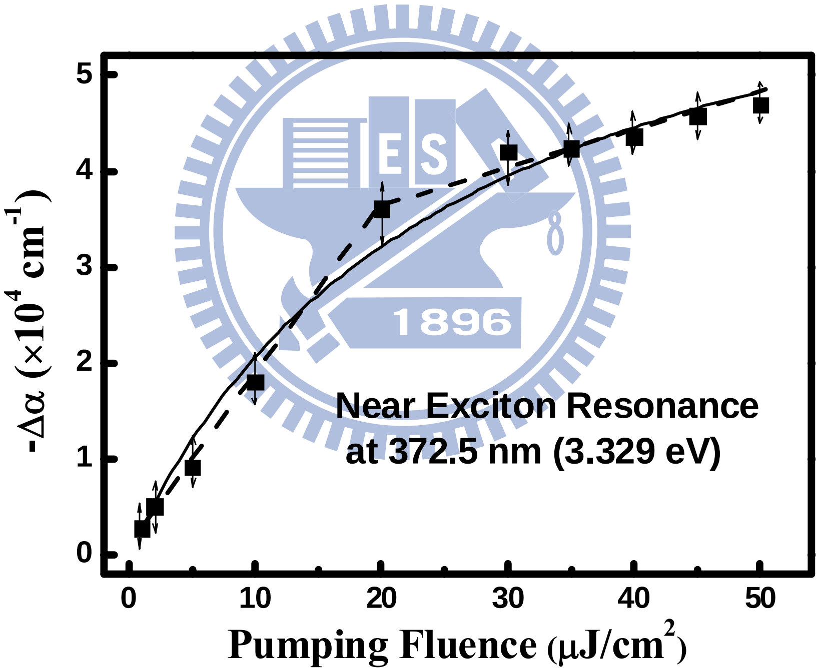

Fig. 5-4. A plot of negative differential absorption maximum as a function of pumping density (solid squares) with excitation near exciton resonance for wavelength at 372.5 nm. The solid curve represents the fitting curve and the dashed lines plotted to guide the eyes revealing a turning point at pumping density of 20 μJ/cm^2.

5.2 Free exciton transient reflectance in the 1-μm ZnO epifilm

5.2.1 Measurement of transient reflectance

When we performed the carrier dynamics near the free exciton transition, the measured transient ΔR/R for the photon energy at 3.298 and 3.281 eV in Fig. 5-5 showed completely different dynamics from those of the above band-gap cases. An instantaneous rising by the pump pulse can be observed at the beginning with no apparent TPA effect. The positive transient differential reflectance quickly decreases and then transits to a negative one followed by a slow recovery.

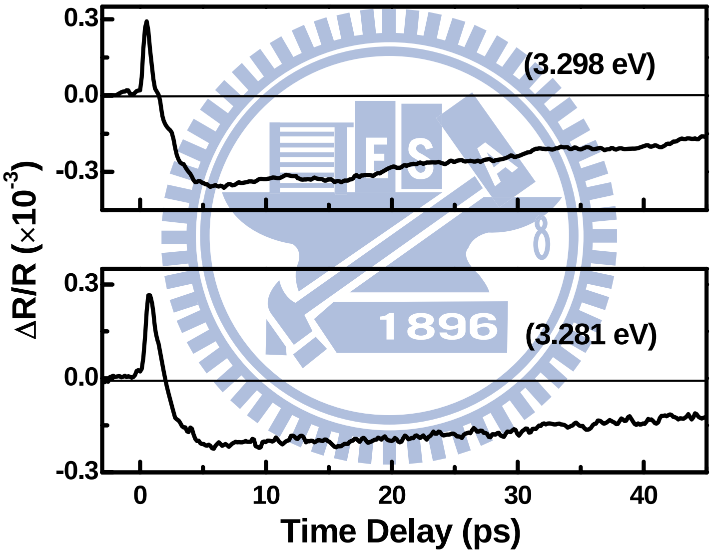

Fig. 5-5. Measurement of transient normalized differential reflectance as a function of time delay for excitation photon energy at 3.298 and 3.281 eV.

For the to best fitting to the temporal traces in Fig. 5-5, we used the response function of bi-exponential decay $a_1\exp(-t/\tau_f) - a_2\exp(-t/\tau_s)$. A fast ($\tau_f$) and a slow ($\tau_s$) decay time constants of 0.8 and 80 ps can be obtained, respectively. Here, we attributed the ultrafast relaxation time (τ_f) to be excitonic thermalization via exciton-phonon scattering. According to the previous time-resolved PL, the free exciton decay time is 75-100 ps in the single ZnO nanowire and 70-90 ps in ZnO bulk [61]. The obtained slow decay time (τ_s) is responsible for the radiative lifetime of free exciton. For excitation energy corresponding to the free exciton transition, the resonantly generated carriers are ionized into free electrons via the assistance of LO-phonon to cause the screening of Coulomb interaction resulting in a reduced band-gap around zero time delay. Then, the excited carriers relax to the lowest energy level via exciton-phonon scattering. After the thermalization process, the excitonic states are occupied by free excitons and the absorption saturation can be achieved by the BF effect at time delay of 4.9 ps.

5.2.2 Model calculation for change of refractive index in ZnO

We plotted the peak amplitude of transient normalized differential reflectance (ΔR/R) at time delay of 0.67 ps as a function of excitation photon energy in Fig. 5-6. It reveals positive ΔR/R for 3.388 eV $< E <$ 3.444 eV and negative ΔR/R for 3.331 $< E <$ 3.388 eV. It is expected that the minimum of ΔR/R will occur around the band-gap energy of 3.354 eV. The differential reflectance (ΔR) can be related to the refractive index change (Δn) resulting from re-distribution of excited carriers after pulse excitation. In the case of ΔR/R << 1, the probed normalized differential reflectance can be described as $\frac{\Delta R}{R} = \frac{4\Delta n}{n^2 - 1}$ [62].

According to previous literature, Bennett et al. [41] proposed a theoretical model, including the BF and BGR effects, to estimate the carrier-induced change of refractive index (Δn) in InP under quasi-equilibrium. These two effects can cause a noticeable change of refractive index especially for near band-edge states. Here, we used this model to calculate the refractive index change induced by the BF (Δn_{BF}) and BGR

(Δn_{BGR}) effects in ZnO, respectively.

The absorption coefficient is assumed to obey a simple square-root law

$$\alpha_0(E) = \begin{cases} \frac{C}{E}\sqrt{E - E_g}\,; E \geq E_g, \\ 0 \qquad\qquad ; E < E_g, \end{cases} \tag{5.2}$$

where C, E, and E_g are the material constant, excitation photon energy, and the band-gap energy, respectively. The differential absorption ($\Delta\alpha$) under optical excitation is induced by the BF and BGR effects. In the case of BF effect, the spectral dependence of $\Delta\alpha_{BF}$ is given by

$$\Delta\alpha_{BF} = \alpha_0(E)\cdot(f_v - f_c - 1) \tag{5.3}$$

with f_v and f_c corresponding to the occupation probabilities of valence and conduction bands having the form of Fermi-Dirac distribution at RT. On the other hand, the differential absorption from BGR effect ($\Delta\alpha_{BGR}$) can be calculated by using the equation of

$$\Delta\alpha_{BGR} = \frac{C}{E}\sqrt{E - E'_g} - \alpha_0(E), \tag{5.4}$$

where $E'_g = E_g - \Delta E_g = E_g - \kappa\cdot\rho^{1/3}$ is the renormalized band-gap energy and ΔE_g represents the reduction of band-gap. In ZnO, κ is the coefficient of band-gap shrinkage on the order of 1.3×10^{-5} meV-cm [63], and ρ is the carrier density. By applying the Kramers-Kronig (K-K) relation to the differential absorption, the BF or BGR induced refractive index change (Δn) can be deduced to be

$$\Delta n(E) = \frac{2c\hbar}{e^2} P\int_0^\infty \frac{\Delta\alpha(E')}{E'^2 - E^2}\, dE', \tag{5.5}$$

where P represents for the Cauchy principle value of the integral.

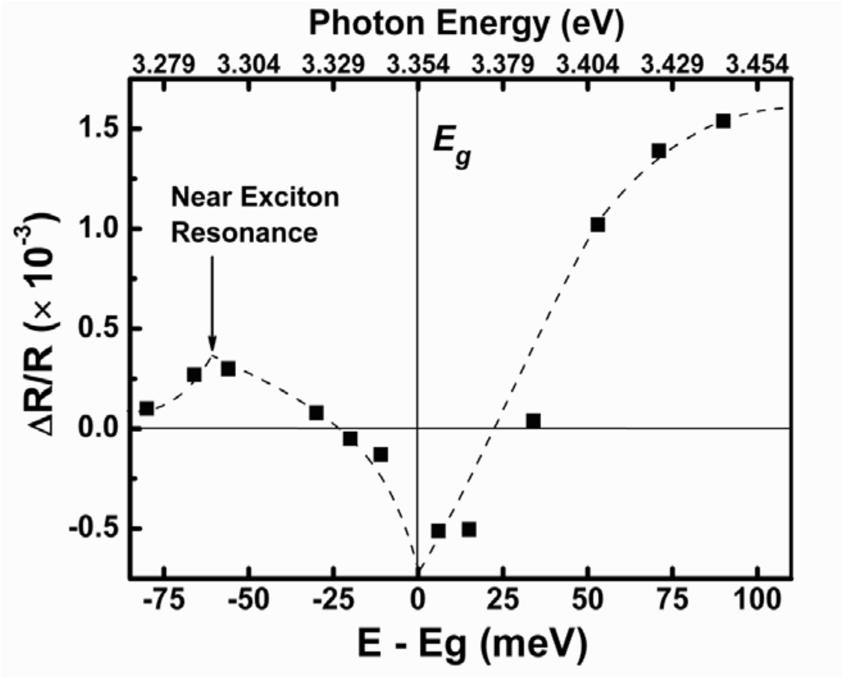

Fig. 5-6. The peak amplitude of measured transient differential reflectance at a time delay of 0.67 ps as a function of excitation photon energy. The dashed lines plotted to guide the eyes.

5.2.3 Spectral dependence of transient reflectance

The excitation carrier density is estimated to be on the order of 2×10^{18} cm^{-3} under excitation fluence of 10 μJ/cm^2 in this work. The spectral dependences of Δn_{BF}, Δn_{BGR} and Δn for ZnO are illustrated in Fig. 5-7 with the carrier density of 1×10^{18} cm^{-3} and 5×10^{18} cm^{-3}. The BF produces a positive index change or $\Delta n_{BF} > 0$ with photon energy above 3.396 eV, and it decreases and transits to negative as the energy approaches E_g. The minimum of Δn_{BF} emerges at the nominal band-gap energy of 3.354 eV. On the other hand, the BGR effect with relatively small spectral dependence leads to a negative index change or $\Delta n_{BGR} < 0$ for the energy above E_g, and it leads to a positive index change for the energy below E_g. The reduction of band-gap energy (ΔE_g) is estimated to be 13 meV. It can be observed that the minimum of Δn_{BGR} and the maximum of Δn_{BGR} are corresponding to the nominal band-gap energy and the renormalized band-gap energy, respectively. The resultant Δn due to the combined effects ($\Delta n_{BF}+\Delta n_{BGR}$) reveals positive for the energy well above E_g, and then becomes negative as the energy approaches E_g.

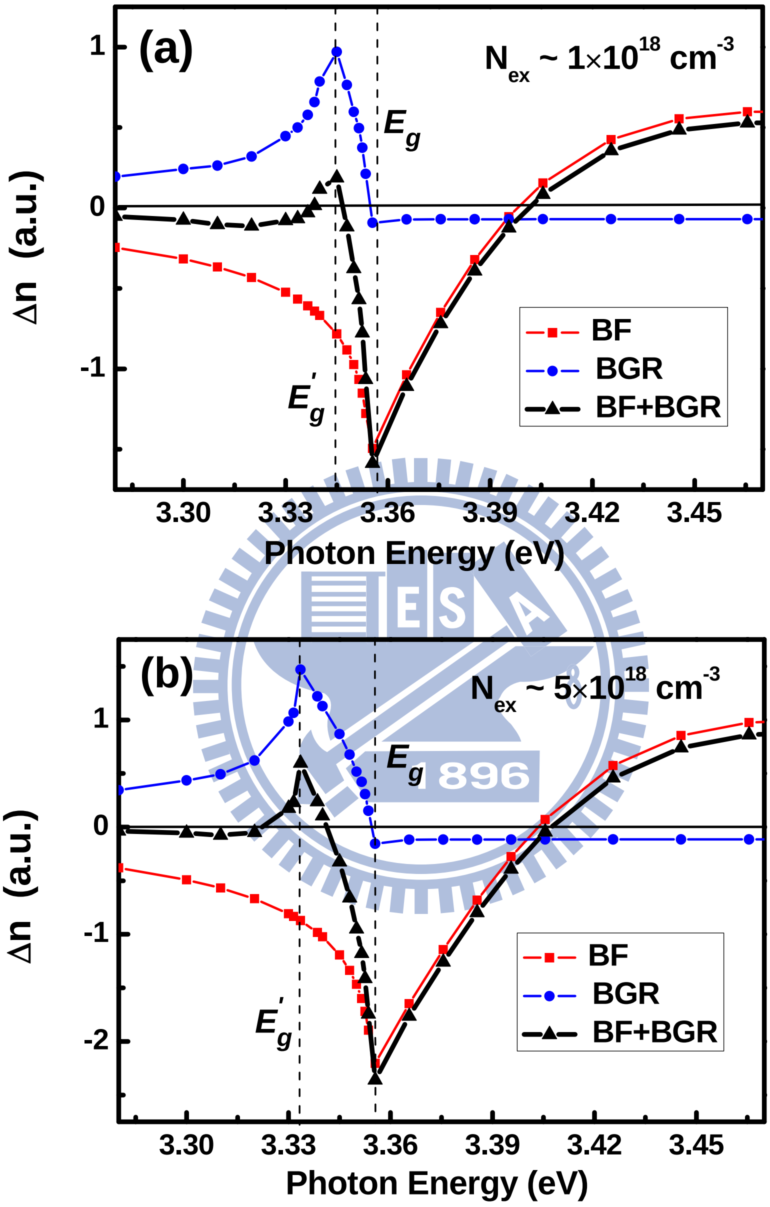

Fig. 5-7. Theoretical calculation of refractive index change in ZnO with spectral dependence by considering the band-filling effect (Δn_{BF}) and the band-gap renormalization effect (Δn_{BGR}). For excited carrier density of (a) 1×10^{18} cm^{-3} and (b) 5×10^{18} cm^{-3}.

By using the equation of $\frac{\Delta R}{R} = \frac{4\Delta n}{n^2 - 1}$, the calculation normalized differential reflectance as a function of photon energy was shown in Fig. 5-8. From the analysis above, the measurement of transient peak reflectance decreases with decreasing the photon energy for excitation above the band-gap states can be explained. As shown in Fig. 5-6, the competition of positive Δn_{BF} over negative Δn_{BGR} yields a positive ΔR/R for $E > 3.388$ eV. The value of ΔR/R approaches to zero for photon energy approaching 3.388 eV, which indicates that Δn contributed from the BF is equal to the value from the BGR effect. Due to Δn induced by the BF becomes negative or smaller than that induced by the BGR effect, it results in a negative ΔR/R for 3.331 eV $< E <$ 3.388 eV. The sign of transient ΔR/R gradually transits to a positive one when we further decrease the excited photon energy. Due to the contribution by near exciton resonance state (~ 3.294 eV), the relatively maximal ΔR/R can be observed for excitation below the band-gap energy. We noticed that the experimental result is somewhat different from the theoretical calculation especially for the photon energy below the band-gap. Due to the limitation of model, we assumed the absorption spectrum by using the square-root rule for the above band-gap states without taking the excitonic state into consideration.

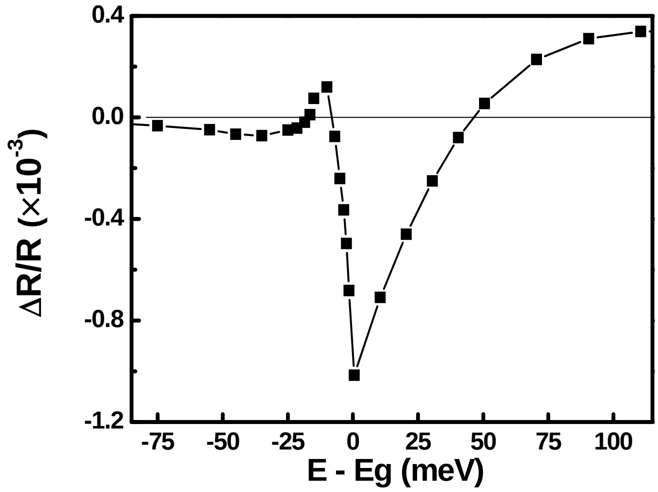

Fig. 5-8. Theoretical calculation of normalized differential reflectance as a function of photon energy.

5.3 Summary

We observed ultrafast free exciton thermalization time of 700-900 fs and obtained the magnitude of maximal differential absorption to be 1.8×10^{4} cm^{-1} with the pumping fluence of 10 μJ/cm^{2} by measuring transient differential transmission in the 70 nm ZnO epitaxial layer at RT. The largest induced transparency occurs near exciton resonance associated with absorption saturation by comparing the excitation from the above band-gap to band-tail states. The pumping dependent dynamics reveals transition of excitonic relaxation from exciton-phonon scattering to exciton-exciton scattering or to an EHP. Moreover, based on a theoretical model to calculate the carrier-induced change of refractive index in ZnO, the measurement of spectral dependent transient reflectance in the 1 μm epifilm can be successfully analyzed as a result of combining effects of band-filling and band-gap renormalization. The measured transient reflectance decreases with decreasing the photon energy for excitation above the band-gap states revealing the significance of competition of the BF and BGR effects.

Chapter 6 Wavelength dependent saturation of one- and two-photon absorptions in ZnO/ZnMgO multiple quantum well structures

Our previous studies in ZnO thin films have shown the enhancement of nonlinear absorption induced by the two-photon exciton resonance with excitation energy of one-half exciton transition energy ($E_{ex}/2$) in the near-IR range [26]. When it was operated in the band-tail region of ZnO thin films, we also found the two-photon absorption (TPA) coefficient can be enhanced as the excitation wavelength approaching the exciton resonance [27]. Fig. 6-1 shows the results of measured two-photon absorption (TPA) coefficient in ZnO in the IR and UV region. However, the contribution of TPA and saturated absorption (SA) to optical nonlinearity in ZnO/ZnMgO MQWs is still unclear. In this chapter, we first demonstrated the wavelength dependent nonlinear absorption in ZnO/ZnMgO MQWs, with excitation from near band-edge toward the shallow band-tail region of QWs, by using the open-aperture Z-scan technique with femtosecond mode-locked laser at RT. Moreover, we performed the intensity dependent measurements to observe the concurrence of SA and TPA characteristics.

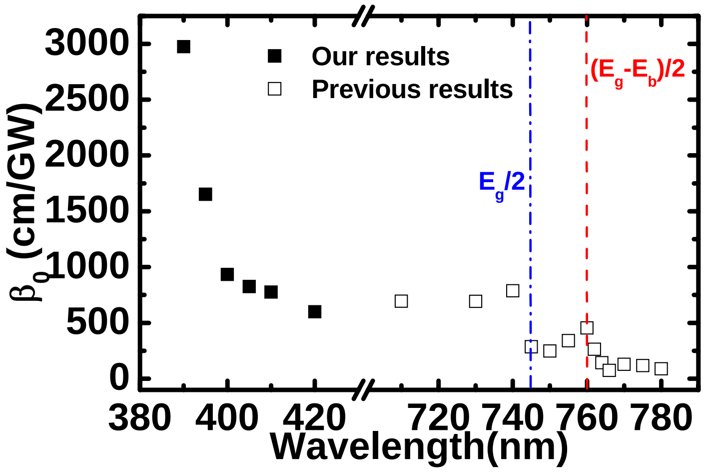

Fig. 6-1. Measurement of two-photon absorption (TPA) coefficient of ZnO with excited photon wavelength in the IR and UV region. [27]

6.1 Spectral dependent two-photon absorption

The measurement of normalized transient differential transmission as a function of time delay for excitation wavelength at 361.5 nm in ZnO/ZnMgO MQWs was shown in the Fig. 6-2, which a negative dip due to the two-photon absorption (TPA) effect around zero time delay can be observed. The observed negative autocorrelation type dips resulted mainly from the process of instantaneous nonlinear absorption by absorbing one pump beam and one probe beam. In order to realize the spectral dependent optical nonlinear absorption, we measured the components of TPA as a function of photon wavelength in ZnO epifilms and ZnO/ZnMgO MQWs as shown in the Fig. 6-3. It can be found that no TPA can be observed for excitation ranging from near-band-edge states to free exciton transition. This is maybe due to the forbidden selection rule that the conduction band-edge is s-wave dominant and the maximum of valence band is p-wave dominant

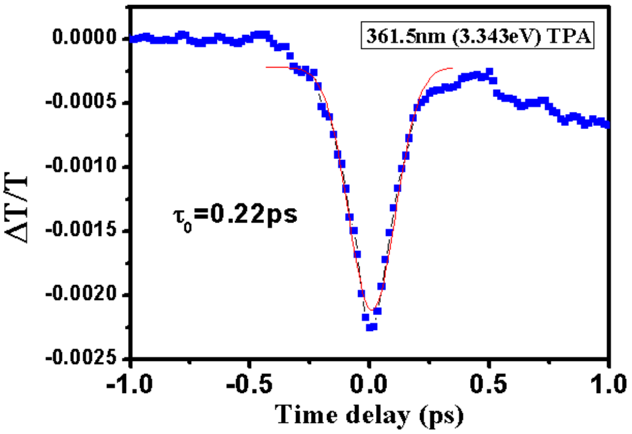

Fig. 6-2. The measured normalized transient differential transmission as a function of time delay for excited wavelength at 361.5 nm in ZnO/ZnMgO MQWs.

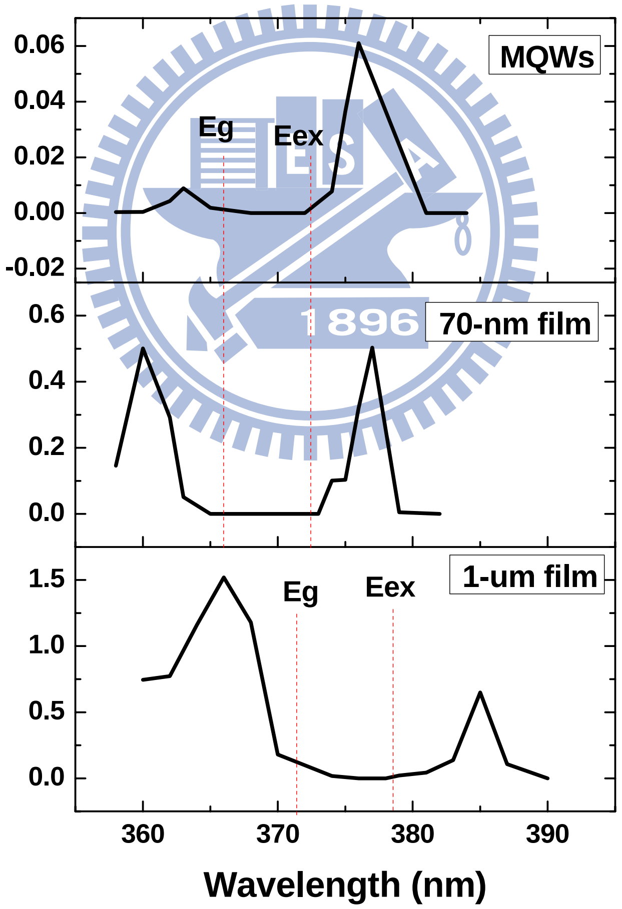

Fig. 6-3. The components of two-photon absorption (TPA) as a function of excitation wavelength in ZnO/ZnMgO MQWs and ZnO epitaxial films.

6.2 Saturated absorption (365 - 373 nm)

In the single beam open-aperture Z-scan experiment, the transmittance of sample is measured as a function of the sample position along the z-axis. The measured normalized transmittance of Z-scan traces for excitation wavelengths at 365, 369 and 373 nm under pumping intensity of 42.5 MW/cm^2 are shown in Fig. 6-4. The results show obvious symmetric peaks at the focal point at z = 0 due to the saturable absorption (SA) induced by the Burstein-Moss effect or the band-filling effect. The SA is a type of nonlinear absorption mechanism, which results in decrease of linear absorption as increasing the input optical intensity. The semiconductor materials with SA properties have been used for generating short pulse laser source [64]. When it was performed with excitation from the near band-edge states (~ 365 nm) to the free exciton transition (~ 373 nm) of ZnO/ZnMgO QWs, the Z-scan traces are similar except that the peak amplitude increases as decreasing the excitation energy approaching the exciton transition. In order to acquire the optical nonlinear absorption coefficients, we consider a beam propagating through a thin nonlinear material. The optical loss inside the sample can be expressed as [45]

$$\frac{dI}{dz'} = -(\alpha_0 + \beta_{eff} I) I \, , \tag{6.1}$$

where α_0 is the linear absorption coefficient, β_{eff} is the effective nonlinear absorption coefficient, and z′ represents the coordinate within the sample. Assuming the incident laser beam has both Gaussian spatial and temporal profiles, Eq. (7.1) can be solved by integrating spatially and temporally to obtain the equation [45]

$$T(z) = \sum_{m=0}^{\infty} \frac{[-\beta_{eff} I_0 L_{eff} / (1 + z^2 / z_0^2)]^m}{(m+1)^{3/2}} \tag{6.2}$$

that can be used to fit the normalized transmittance of the measured open-aperture Z-scan trace. Here I_0 is the on-axis pumping intensity, $L_{eff} = [1-\exp(-\alpha_0 L)]/\alpha_0$ is the effective interaction length, and z_0 is the Rayleigh range. The fitted results reveal the nonlinear absorption coefficients β_{eff} = -768, -2215, -3337 and -4450 cm/MW for excited photon wavelengths at 365, 369, 371 and 373 nm, respectively. The largest magnitude of β_{eff} can be deduced at 373 nm that indicates enhancement of the nonlinear absorption at near exciton resonance associated with absorption saturation. We also performed the open-aperture Z-scan in a thin ZnO epitaxial layer for comparison, not shown in the figures, that also shows the SA property with β_{eff} = -2372 cm/MW at near exciton resonance under intensity of 42.5 MW/cm^2.

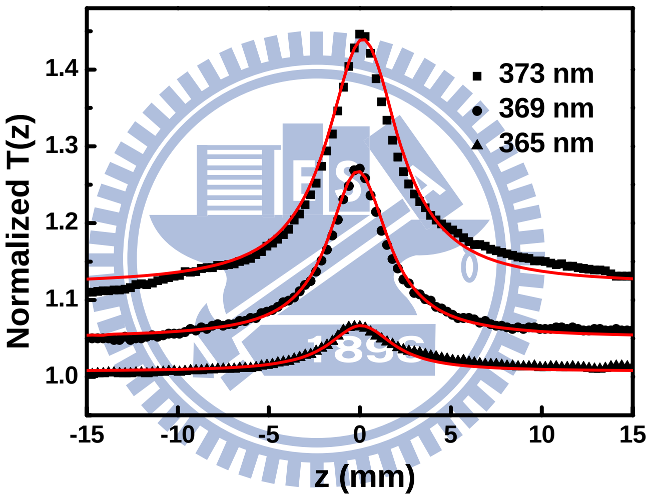

Fig. 6-4. Normalized transmittance of open-aperture Z-scan traces for excited photon wavelength at 365, 369 and 373 nm. The symbols are experimental data and the solid lines are theoretically fitting curves. Traces are vertically displaced for clarity.

In order to investigate the nonlinear absorption properties near exciton resonance, we performed the intensity dependent Z-scan experiments for excitation wavelength at 373 nm with input pumping intensity ranging from 51 to 170 MW/cm^2. As shown in Fig. 6-5, all the Z-scan traces exhibit SA and the normalized transmittance at $z = 0$ increases with increasing the pumping intensity. To fit the intensity dependent open-aperture Z-scan traces in Fig. 6-5, the optical loss inside the sample was expressed as:

$$\frac{dI}{dz'} = -\frac{\alpha_0}{1+I/I_S} I . \tag{6.3}$$

Due to the symmetry and the large density of states (DOS) near exciton resonance, the contribution to the nonlinear response mainly results from the SA for excitation wavelength at 373 nm. We obtained the fitting parameters of α_0 and I_S to be 6.8×10^5 cm^{-1} and 137 ± 4 MW/cm^2, respectively.

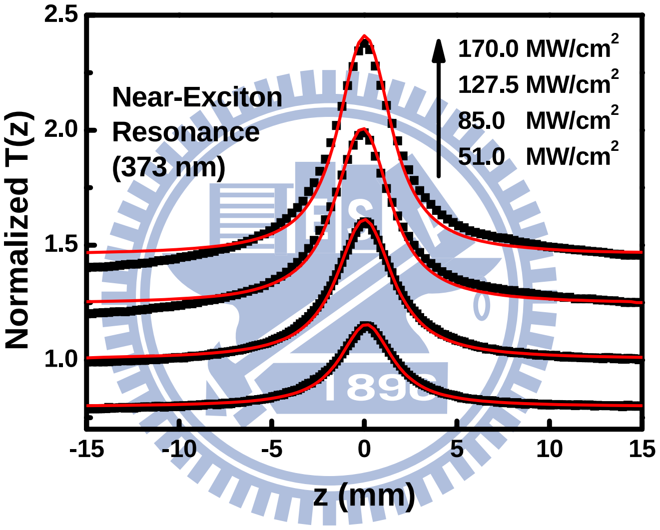

Fig. 6-5. Normalized transmittance of open-aperture Z-scan traces near exciton resonance with excitation intensity ranging from 51 to 170 MW/cm^2. Traces are vertically displaced for clarity.

6.3 Saturated absorption (SA) versus two-photon absorption (TPA)

As we further decrease the excitation energy to the band-tail region, the measured open-aperture Z-scan traces for excitation wavelength at 375 and 378 nm are shown in Fig. 6-6. The Z-scan traces reveal the simultaneous occurrence of SA and two-photon absorption (TPA) for excitation wavelength at 375 nm. The TPA as a kind of nonlinear absorption mechanism involves a transition from ground state to high energy level by simultaneously absorbing two excited photons, which causes the reduction of transmittance as increasing the pumping intensity. We found the nonlinear response gradually switches from the TPA to the SA as increasing the pumping intensity for photon wavelength at 375 nm. Moreover, the Z-scan traces reveal obvious symmetric dip around the focal point for excitation wavelength at 378 nm. It can be observed that the nonlinear response shows the TPA along with saturation of TPA as increasing the pumping intensity. In order to fit the intensity dependent open-aperture Z-scan traces in Fig. 6-6, the optical loss inside the sample was expressed as the combination of SA and saturation of TPA that had been used to analyze the nonlinear absorption characteristics of amorphous InSe thin films [65]:

$$\frac{dI}{dz'} = -\left(\frac{\alpha_0}{1 + I/I_S} + \frac{\beta I}{1 + I^2/I_S^2}\right)I, \tag{6.4}$$

where α_0 is the linear absorption constant, β and I_S represent the TPA coefficient and the saturation intensity, respectively.

For excitation wavelength at 375 nm, where SA and TPA occur simultaneously, the first and second terms in Eq. (6.4) compete to each other in determining the magnitude and the signature of nonlinear response. On the other hand, the Z-scan traces exhibit dominance of TPA accompanied with small contribution from SA for excitation wavelength at 378 nm, which is on the lower energy side of shallow band-tail region. From the theoretical fitting, the TPA coefficient (β) and the saturation intensity (I_S) were obtained to be 3653 cm/MW and 162 MW/cm^2, respectively, for photon wavelength at 375 nm. In addition, we obtained β = 2380 cm/MW and I_S = 128 MW/cm^2 for photon wavelength at 378 nm. The measured parameters of nonlinearities in ZnO/ZnMgO MQWs will be useful to design the optical limiting devices and optical switching elements. From our previous reports in ZnO thin films, the value of TPA coefficient increases from 0.6 cm/MW for photon wavelength at 420 nm to 3 cm/MW at 390 nm [27]. Irimpan et al. [66] have measured the TPA coefficient of 1.17 cm/MW in ZnO colloids. On the other hand, Gu et al. [67] have observed the TPA saturation resulting from the interband two-photon transition in II–VI semiconductors, such as CdS, CdSe, and ZnSe, in which the saturation intensity was obtained to be on the order of 5 GW/cm^2 under femtosecond laser excitation.

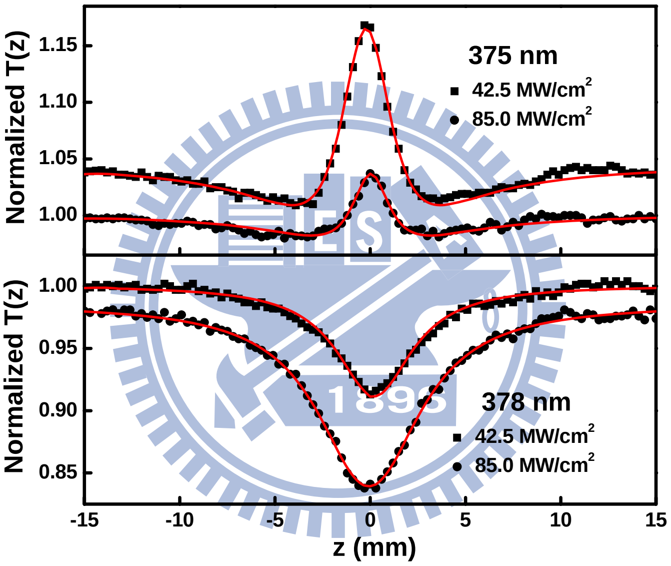

Fig. 6-6. Normalized transmittance of open-aperture Z-scan traces for photon wavelength at (a) 375 nm and (b) 378 nm with excitation intensity of 42.5 and 85 MW/cm^2. Traces are vertically displaced for clarity.

6.4 Summary

The wavelength and intensity dependent nonlinear absorption was demonstrated in ZnO/ZnMgO multiple quantum wells (MQWs) by utilizing the Z-scan method at room temperature. The saturation of one-photon absorption (OPA) increases as the excitation photon energy approaches the free exciton transition of ZnO QWs from the conduction bandedge, while the two-photon absorption (TPA) is minimal. The maximal nonlinear absorption coefficient is -4450 cm/MW at the exciton resonance. The contribution of TPA increases as tuning excitation in the shallow band-tail region, therefore, we used a phenomenological model of combining saturation of OPA and TPA to analyze the intensity dependent Z-scan traces. The characteristics of nonlinear absorption reveal the concurrence of saturation of OPA and TPA for excitation wavelength at 375 nm, and gradually transit to the dominance of TPA as further decreasing the excitation energy to the photon wavelength at 378 nm.

Chapter 7 Conclusion

7.1 Conclusion

In this thesis, we investigated the spectral-, thickness- and pumping-dependent ultrafast thermalization of free carriers and excitons in ZnO epitaxial thin films by using the degenerate pump-probe technique at room temperature. The measurement of spectral dependent transient reflectance shows that the ultrafast thermalization time increases slightly with increasing the excited photon energy for above band-gap states. The free carrier thermalization is due to the carrier and optical-phonon scattering for well above band-gap states; while it is mainly due to the carrier and acoustic-phonon scattering for near band-edge states with an excess energy less than 26 meV. Moreover, based on a theoretical model by considering the combination of band-filling and band-gap renormalization (BGR) effects, we calculated the change of refractive index (Δn) in ZnO to successfully explain the measured spectral dependent transient reflectance.

The thickness effect on ultrafast thermalization of free carriers in above band-gap states was performed by conducting the free carrier dynamics in a thin and a thick ZnO epilayers, corresponding to the thickness of 70 nm and 1 μm, respectively. The far above band-gap dynamics in a 70 nm sample reveals the prolonged thermalization time of 10 ps and the slow recovery of renormalized band-gap. When performed in a thin sample, the interaction between free carriers and sample surface can induce the loss of excited carrier density to result in the decrease of BGR effect. In addition, the loss of excited carrier density via surface trapping effect results in the inefficient carrier-phonon scattering and the energy dependent BGR build-up time. However, the ultrafast thermalization time in a 1 μm epifilm was obtained to be on the order of 1.0-1.4 ps due to the surface trapping effect can be ignored in a thick sample. Both of thin and thick samples reveal the ultrafast thermalization for near band-edge states.

By measuring the transient differential transmission under exciton resonant excitation, we demonstrated the transient absorption for free exciton transition. We obtained the ultrafast relaxation time less than 1 ps and the magnitude of maximal differential absorption coefficient ($\Delta\alpha$) to be 1.8×10^{4} cm^{-1} with pumping fluence of 10 μJ /cm^{2}. The relaxation time decreases with increasing the pumping fluence, which indicates the transition of excitonic relaxation from the exciton-phonon scattering to the exciton-exciton scattering or to an electron-hole plsma (EHP). By comparing the measurement of transient transmission spectrum with excitation from above band-gap states to band-tail states, the largest induced transparency associated with absorption saturation can be observed at near exciton resonance.

In addition to the investigation of ultrafast spectral phenomena in ZnO epitaxial films, we also utilized the standard open-aperture Z-scan technique to realize the optical properties of nonlinear absorption in ZnO/ZnMgO multiple quantum well structures (MQWs). The saturation of one-photon absorption (OPA) can be observed with excitation photon energy from the conduction band-edge approaching the free exciton transition in ZnO QWs. The maximal nonlinear absorption coefficient occurs at near exciton resonance associated with absorption saturation. The contribution of the two-photon absorption (TPA) emerges as tuning the excitation in the shallow band-tail region. The characteristics of nonlinear absorption reveal the concurrence of OPA and TPA saturation for excitation wavelength at 375 nm, and gradually transit to the dominance of TPA saturation for excitation wavelength at 378 nm.

7.2 Prospective

For the purpose of more complete femtosecond time-resolvd equipment, the non-degenerate optical pump-probe system can be achieved by using the mode-locked Ti:sapphire laser and photonic crystal fiber (PCF) to generate the super continuum probe beam for transient absorption spectroscopy. Not only the transient absorption measurement, the setup femtosecond resolved TRPL system, such as the up-conversion method as shown in Fig. 7-1 [68], will be useful to study the optical gain and lasing dynamics in ZnO-related materials.

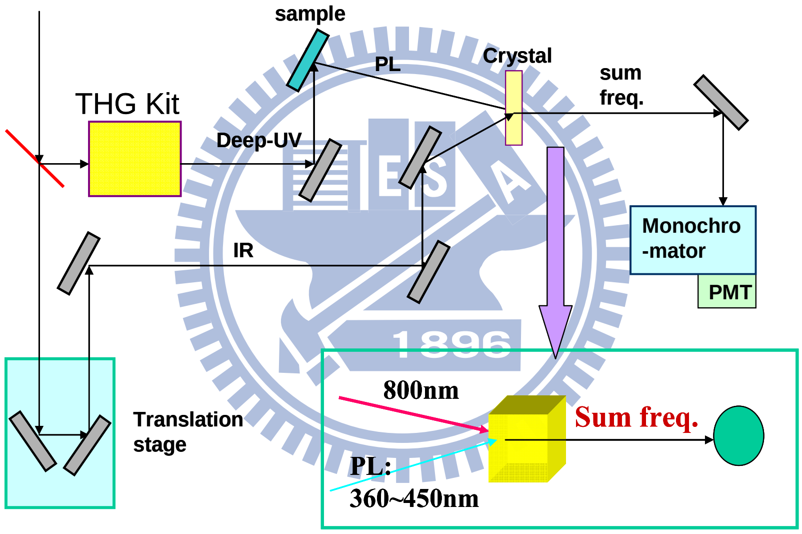

Fig. 7-1. The setup of Up-conversion method for femtosecond resolved TRPL system.

Our groups have found that the strength of exciton and LO-phonon coupling can be reduced in ZnO quantum dots as shown in Fig. 7-2 [69]. In addition, the excitons in ZnO/ZnMgO QWs exhibit strong stability as compared to bulk material due to the enhancement of exciton binding energy and the reduction of exciton-phonon coupling when the scale of ZnO-related nanostructures is close to exciton Bohr radius. Therefore, it is interesting to observe the quantum confinement effect by investigating the ultrafast carrier dynamics in ZnO/ZnMgO MQWs with well-width or barrier-width dependence.

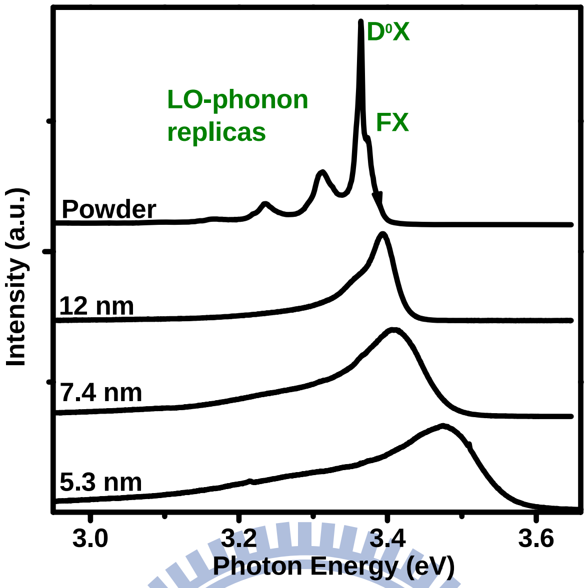

Fig. 7-2. Low temperature PL spectra at 13K in size controlled ZnO quantum dots.

References

[1] Y. F. Chen, D. M. Bagnall, H. J. Koh, K. T. Park, K. Hiraga, Z. Q. Zhu and T. Yao, J. Appl. Phy. 84 3912 (1998).

[2] Z. K. Tang, G. K. L. Wong, P. Yu, M. Kawasaki, A. Ohtomo, H. Koinuma and Y. Segawa, Appl. Phys. Let. 72, 3270 (1998).

[3] P. Zu, Z. K. Tang, G. K. L. Wong, M. Kawasaki, A. Ohtomo, H. Koinuma and Y. Swgawa, Solid State Commun. 103, 459 (1997).

[4] T. Makino, C. H. Chia, N. T. Tuan, Y. Segawa, M. Kawasaki, A. Ohtomo, K. Tamura and H. Koinuma, Appl. Phys. Lett. 76 3549 (2000).

[5] D. C. Look, Materials Science and Engineering B 80, 383 (2001).

[6] Ü. Özgür, Ya. I. Alivov, C. Liu, A. Teke, M. A. Reshchikov, S. Doğan, V. Avrutin, S. J. Cho and H. Morkoç, J. Appl. Phys. 98, 041301 (2005).

[7] T. H. Moon, M. C. Jeong, W. Lee and J. M. Myoung, Appl. Surf. Sci. 240, 280 (2005).

[8] N. Ohashi, K. Kataoka, T. Ohgaki, T. Miyagi, H. Haneda and K. Morinaga, Appl. Phys. Lett. 83, 4857 (2003).

[9] P. Sharma, S. Kumar and K. J. Sreenivas, Mater. Res., 18, 545 (2003).

[10] Q. Wan, C. L. Lin, X. B. Yu, and T. H. Wang, Appl. Phys. Lett., 84, 124 (2004).

[11] R. Katoh, A. Furube, K. Hara, S. Murata, H. Sugihara, H. Arakawa, and M. Tachiya, J. Phys. Chem. B, 106, 12957 (2002).

[12] C. Klingshirn, Semiconductor Optics, Springer, (2005).

[13] R. T. Senger, and K. K. Bajaj, Phys. Rev. B 68, 045313 (2003).

[14] D.M. Bagnall, Y.F. Chen, M.Y. Shen, Z. Zhu, T. Goto and T. Yao, J. Crystal Growth 184, 605 (1998).

[15] W. Gcpel, U. Lampe, Phys. Rev. B 22, 6447 (1980).

[16] D. M. Bagnall, Y. F. Chen, Z. Zhu, T. Yao, S. Koyama, M. Y. Shen and T. Goto,

Appl. Phys. Lett. 70, 2230 (1997).

[17] D. M. Bagnall, Y. F. Chen, Z. Zhu, T. Yao, M. Y. Shen and T. Goto, Appl. Phys. Lett. 73, 1038 (1998).

[18] Y. Sun, J. B. Ketterson and G. K. L. Wong, Appl. Phys. Lett. 77, 2322 (2000).

[19] S. P. Lau, H. Y. Yang, S. F. Yu, H. D. Li, M. Tanemura, T. Okita, H. Hatano and H. H. Hng, Appl. Phys. Lett. 87, 013104 (2005).

[20] J. C. Johnson, H. Yan, P. Yang and R. J. Saykally, J. Phys. Chem. B 107, 8816 (2003).

[21] J. Takeda, S. Kurita, Y. Chen and T. Yao, Int. J. Modern Phys. B 15, 3669 (2001).

[22] Ü. Özgür, A. Teke, C. Liu, S. J. Cho, H. A. Morko and H. O. Everitt, Appl. Phys. Lett. 84, 3223 (2004).

[23] A. B. Djurišić, W. M. Kwok, Y. H. Leung, W. K. Chan and D. L. Phillips, J. Phys. Chem. B 109, 19228 (2005).

[24] A. Teke, Ü. Özgür, S. Doğan, X. Gu and H. Morkoçd, Phys. Rev. B 70, 195207 (2004).

[25] J. F. Muth, R. M. Kolbas, A. K. Sharma, S. Oktyabrsky and J. Narayan, J. Appl. Phys. 85, 7884 (1999).

[26] J. H. Lin, Y. J. Chen, H. Y. Lin and W. F. Hsieh, J. Appl. Phys. 84, 3912 (2005).

[27] Y. P. Chan, J. H. Lin, C. C. Hsu and W. F, Hsieh, Optics Express 16, 19900 (2008).

[28] T. J. Schmidt, J. J. Song, Y. C. Chang, R. Horning and B. Goldenberg, Appl. Phys. Lett. 72, 1504 (1998).

[29] C. K. Sun, J. C. Liang, X. Y. Yu, S. Keller, U. K. Mishra and S. P. DenBaars, Appl. Phys. Lett. 78, 2724 (2001).

[30] S. Hess, R. A. Taylor, K. Kyhm, J. F. Ryan, B. Beaumont and P. Gibart, Phys. Sstatus Solidi B 216, 57 (1999).

[31] A. Yamamoto, T. Kido, T. Goto, Y. F. Chen, T. Yao and A. Kasuya, Appl. Phys. Lett. 75, 469 (1999).

[32] C. K. Sun, S. Z. Sun, K. H. Lin, K. Y. J. Zhang, H. L. Liu, S. C. Liu and J. J. Wu, Appl. Phys. Lett. 87, 023106 (2005).

[33] J. Takeda, H. Jinnouchi, S. Kurita, Y. F. Chen and T. Yao, Phys. Status Solidi (b) 229, 877 (2002).

[34] Y. Toshine, J. Takeda, H. J. Ko and T. Yao, Phys. Status Solidi (c) 1, 839 (2004).

[35] J. Fallert, F. Stelzl, H. Zhou, A. Reiser, K. Thonke, R. Sauer, C. Klingshirn and H. Kalt, Opt. Express 16, 1125 (2008).

[36] T. Koida, A. Uedono, A. Tsukazaki, T. Sota, M. Kawasaki and S. F. Chichibu, Phys. Status Solidi (a) 201, 2841 (2004).

[37] K. T. Tsen, "Ultrafast Physical Processes in Semiconductors", Academic Press, (2001).

[38] J. Shah, "Ultrafast Spectroscopy of Semiconductors and Semiconductor Nanostructures", Springer-AT&T, Berlin, (1996).

[39] M. A. Stroscio and M. Dutta, "Phonons in Nanostructures", Cambridge, (2001).

[40] R. R. Alfano, "Semiconductors Probed by Ultrafast Laser Spectroscopy", Academic Press, (1984).

[41] B. R. Bennett, R. A. Soref and J. A. Del Alamo, IEEE J. Quantum Electron. 26, 113 (1990).

[42] J. Takeda, K. Nakajima, S. Kurita, S. Tomimoto, S. Saito and T. Suemoto, Phys. Rev. B 62, 10083 (2000).

[43] W. R. Liu, W. F. Hsieh, C. H. Hsu, K. S. Liang and F. S. S. Chien, J. Crystal Growth 297, 294 (2006).

[44] B. Guo, Z. R. Qiu, J. Y. Lin, H. X. Jiang and K. S. Wong, Appl. Phys. B 80, 521 (2005).

[45] M. Sheik-Bahae, A. A. Said, T. H. Wei, D. J. Hagan and E. W. Van Stryland, IEEE J. Quantum Electron. 26, 760 (1990).

[46] W. Y. Liang and A. D. Yoffe, Phys. Rev. Lett. 20, 59 (1968).

[47] C. Klingshirn, R. Hauschild, J. Fallert and H. Kalt, Phys. Rev. B 75, 115203 (2007).

[48] C. Klingshirn, Phys. Stat. Sol. (b) 244, 3027 (2007).

[49] K. H. Lin, G. W. Chern, Y. C. Huang, S. Keller, S. P. DenBaars and C. K. Sun, Appl. Phys. Lett. 83, 3087 (2003).

[50] C. K. Sun, F. Vallee, S. Keller, J. E. Bowers and S. P. DenBaars, Appl. Phys. Lett. 70, 2004 (1997).

[51] J. Takeda, N. Arai, Y. Toshine, H. J. Ko and T. Yao, Japan. J. Appl. Phys. 45, 6961 (2006).

[52] W. M. Kwok, A. B. Djurišić, Y. H. Leung, W. K. Chan and D. L. Phillips, Appl. Phys. Lett. 87, 223111 (2005).

[53] A. Othonos, J. Appl. Phys. 83, 1789 (1998).

[54] Y. F. Chen, N. T. Tuan, Y. Segawa, H. J. Ko, S. K. Hong and T. Yao, Appl. Phys. Lett. 78, 1469 (2001).

[55] T. Koida, A. Uedono, A. Tsukazaki, T. Soto, M. Kawasaki and S. F. Chichibu, Phys. Stat. Sol. (a) 201, 2841 (2004).

[56] Y. Toshine, J. Takeda, H. J. Ko and T. Yao, Phys. Stat. Sol. (c) 1, 839 (2004).

[57] W. H. Knox, R. L. Fork, M. C. Downer, D. A. B. Miller, D. S. Chemla, C. V. Shank, A. C. Gossard and W. Wiegmann, Phys. Rev. Lett. 54, 1306 (1985).

[58] P. C. Becker, D. Lee, A. M. Johnson, A. G. Prosser, R. D. Feldman, R. F. Austin and R. E. Behringer, Phys. Rev. Lett. 68, 1876 (1992).

[59] S. W. Koch, N. Peyghambarian and M. Lindberg, J. Phys. C 21, 5229 (1988).

[60] Y. Wang, A. Suna, J. McHugh, E. F. Hilinski, P. A. Lucas and R. D. Johnson, J.

Chem. Phys. 92, 6927 (1990).

[61] J. C. Johnson, K. P. Knutsen, H. Yan, M. Law, Y. Zhang, P. Yang and R. J. Saykally, Nnao Lett. 4, 197 (2004).

[62] A. J. Sabbah and D. M. Riffe, Phys. Rev. B 66, 165217 (2002).

[63] J. D. Ye, S. L. Gu, S. M. Zhu, S. M. Liu, Y. D. Zheng, R. Zhang and Y. Shi, Appl. Phys. Lett. 86, 192111 (2005).

[64] A. M. Fox, A. C. Maciel, M. G. Shorthose, J. F. Ryan, M. D. Scott, J. I. Davies and J. R. Riffat, Appl. Phys. Lett. 51, 30 (1987).

[65] M. Yuksek, U. Kurum, H. G. Yaglioglu, A. Elmali and A. Ates, J. Appl. Phys. 107, 033115 (2010).

[66] L. Irimpan, A. Deepthy, B. Krishnan, V. P. N. Nampoori and P. Radhakrishnan, Appl. Phys. B 90, 547 (2008).

[67] B. Gu, Y. X. Fan, J. Chen, H. T. Wang, J. He and W. Ji, J. Appl. Phys. 102, 083101 (2007).

[68] A. Yamamoto, T. Kido, T. Goto, Y. F. Chen, T. F. Yao and A. Kasuya, J. Crystal Growth 214, 308 (2000).

[69] W. T. Hsu, K. F. Lin and W. F. Hsieh, Appl. Phys. Lett. 91, 181913 (2007).

個人簡歷

基本資料:

姓名: 歐博濟 (Po-Chi Ou)

性別: 男

出生年月日: 1979 年 11 月 23 日

出生地: 高雄市

通訊處: 高雄市左營區左營大路 301 巷 12 號

Email: inphase.eo94g@nctu.edu.tw

學經歷:

國立高雄師範大學物理學系 學士 (1998/09 ~ 2002/06)

高雄市立三民國中 實習教師 (2002/07 ~ 2003/06)

國立中央大學光電科學研究所 碩士 (2003/09 ~ 2005/06)

國立交通大學光電工程研究所 博士 (2005/09 ~ 2011/09)

Publication list

Journal publications

1. **Po-Chi Ou**, Ja-Hon Lin, Chi-An Chang, Wei-Rein Liu and Wen-Feng Hsieh, "Thickness effect on ultrafast thermalization of carriers in above-band-gap states in ZnO epitaxial films", J. Phys. D: Appl. Phys. **43**, 495103 (2010).
2. **Po-Chi Ou**, Wei-Rein Liu, Ho-Jei Ton, Ja-Hon Lin and Wen-Feng Hsieh, "Ultrafast relaxation and absorption saturation at near exciton resonance in a thin ZnO epilayer", J. Appl. Phys. **109**, 013102 (2011).
3. **Po-Chi Ou**, Ja-Hon Lin and Wen-Feng Hsieh, "Spectral dependence of transient reflectance in a ZnO epitaxial film at room temperature", Accepted for publication in Appl. Phys. B - Lasers and Optics, (2011/07/25).

International conferences

1. **Po-Chi Ou**, Ja-Hon Lin, Chi-An Chang, Wei-Rein Liu and Wen-Feng Hsieh, "Carrier dynamics of thin ZnO epifilm above band-gap states", Poster at 8th Pacific Rim Conference on Lasers and Electro-Optics, (2009/08).
2. **Po-Chi Ou**, Ja-Hon Lin, Chin-Chia Kuo and Wen-Feng Hsieh, "Optical nonlinear absorption of ZnO/ZnMgO multiple quantum wells at room temperature", Poster at IQEC/CLEO Pacific Rim 2011, NO. 3700-PO-109.